Determination of REE in uranium bearing-material for nuclear forensics purposes using ICP-MS

K Seemela

orcid.org/0000-0002-2725-5471

Mini-Dissertation accepted in partial fulfilment of the requirements for the degree of Masters in Applied Radiation Sciences and Technology at the

North West University

Supervisor: Dr TG Kupi

Graduation: July 2023

Student number: 27967344

DECLARATION

I, Kgabo Seemela, hereby declare that this dissertation, which I herewith submit to the North-West University as partial completion of the requirements set for the Master of Science in Applied Radiation Science and Technology degree, is my work and it hasn't been submitted to any other university.

Signed by student .... **…28 November 2022**

Kgabo Seemela **Date**

Signed by Supervisor **…28 April 2023**

Dr. TG Kupi

Signed by Co-Supervisor **…28 November 2022**

Dr. ND Mokhine

ACKNOWLEDGEMENT

I would like to thank God first and foremost for providing me strength during all the challenging parts of accomplishing this dissertation. I want to express my sincere gratitude to my research supervisor, Dr. Mokhine ND, for all of her assistance and guidance throughout the research project. Without her help, this project would not have been achieved. I also like to thank Dr. Kupi TG, my research co-supervisor, for helping me with my lab work and thesis write-up. A special thanks goes out to Mr. Mathapo M for helping me with my statistical analysis. Additionally, I want to thank Mr. Oluwaseji J, Ms Mbele KS, Mr Radebe M and Ms Kgantsi T for helping me with my project and supporting me all the time. I would also acknowledge support from Koena Seemela. My parents: Seemela David & Seemela Jaqueline deserve the most thanks for being there always and praying for me during this difficult journey.

Furthermore, I would like to thank NRF general scholarship 2021/2022 for their financial assistance with my research; without their support, this study could not have been accomplished.

The Centre for Applied Radiation Science and Technology at North-West University deserves special recognition for giving me the chance to conduct my research there.

ABSTRACT

Nuclear forensics is a scientific discipline that focuses on nuclear or radioactive material and aims to provide information on the intended use, history, and even origin of the material. It examines and evaluates the signatures in nuclear and other radioactive materials to assist in criminal investigations involving these materials. The information obtained from forensic investigations needs to be accurate and precise for the evidence to be accepted in court. By using inductively coupled plasma mass spectrometry (ICP-MS), a new and straightforward analytical method has been created for the detection of lanthanides (rare-earth elements) in uranium ore and Uranium Ore Concentration. Rare earth elements (REE), called lanthanides, show consistent patterns under a variety of geochemical conditions. The aim of this project was to determine REE in uranium bearing material for nuclear forensics purposes using ICP-MS. The TRU^{TM} resin was used for a selective extraction chromatographic separation of lanthanides, which was followed by ICP-MS analysis. To improve ionization efficiencies for determining REE concentrations, the chemical separation strategy was intended to limit matrix effects. Four (4) UOC and two (2) uranium ore samples from Witwatersrand basin in South Africa were subjected to the technique to measure REE abundances. Ce/Ce*, Eu/Eu*, La_N/Yb_N, La_N/Gd_N, and Gd_N/Yb_N were the few element ratios that seem to contain substantial information regarding sources. According to the findings, the total REEs (ΣREE) concentrations in several UOC samples were in the following order: UOC4 (15634,541 ppb) > UOC2 (983,972 ppb) > UOC1 (390,182 ppb) > UOC3 (182,968 ppb). For uranium ore samples, the ΣREE concentrations were: U ore1 (12486,420 ppb) > U ore2 (8413,640 ppb). While UOC1, UOC2, and UOC3 of the normalized REE/Cl chondrites pattern of UOC exhibited light rare earth elements (LREE) enrichment and heavy rare earth elements (HREE) depletion with positive Cerium anomalies and negative Europium anomalies, UOC4 demonstrated the opposite, with depletion LREE and HREE enrichment with a large negative Europium anomaly. The enrichment of the medium REEs was more pronounced than that of the LREEs and HREEs. U ore1 and U ore2 indicated positive Ce anomalies and negative Eu anomalies, as shown in the normalized REE/Cl chondrites pattern and their ratios of (La_N/Gd_N) and (Gd_N/Yb_N), ranged from 0.932 to 3.665 and 1.383 to 3.919 respectively. To evaluate their statistical significance in the observed variations, REEs for UOC and uranium ore samples were determined from the acquired data and subjected to ANOVA. The findings showed that among the analysed mining sites, REEs used to determine origin location, exhibited significant variation. It has been proven that these techniques can precisely measure the REE concentration of well-characterized UOC and uranium ore samples. The REE pattern was utilized for the

identification and origin assessment of UOC and uranium ore samples. By doing so, it is simple to confirm the source of an unknown substance by comparing the pattern to that of a known sample. The provenance of the material can also be determined in numerous circumstances even when there is no reference sample available due to characteristic patterns, in contrast to other indicators utilized for nuclear forensic research. Finally, the findings provided in this dissertation can be a helpful tool for forensic nuclear investigations, supporting the fight against the illicit trafficking of nuclear materials.

Keywords: Rare Earth Elements, UOC, Uranium Ore, ICP-MS, ANOVA

LIST OF FIGURES

LIST OF TABLES

LIST OF ABBREVIATIONS

ANOVA	Analysis of variance
CA	Cluster analysis
DRC	Dynamic reaction cell
FTIR	Fourier-transform infrared spectrometry
GDMS	Glow discharge mass spectrometry
GS-EIMS	Gas source electron impact ionisation mass spectrometry
HREE	Heavy rare earth element
IAEA	International Atomic Energy Agency
IC	Internal conversion
ICP-MS	Inductively coupled plasma mass spectroscopy
ISL	In-situ leaching
ITDB	Incident and trafficking database
LREE	Light rare earth element
MORC	Material out of regulatory control
MREE	Medium rare earth element
MS	Mass spectrometry
NFL	Nuclear forensic library
NNFL	National nuclear forensic library
PCA	Principal component analysis
PTFE	Polytetrafluoroethylene
PUREX	Plutonium and uranium extraction
REE	Rare earth element

SAPS	South Africa Police Service
SEM	Scanning electron microscopy
SIMS	Secondary ion mass spectrometry
TIMS	Thermal ionization mass spectrometry
UOC	Uranium ore concentrate
WCA	Wonderfonteinspruit catchment area
XRD	X-ray diffraction

Table of Contents

CHAPTER 1: INTRODUCTION AND PROBLEM STATEMENT

1.1 Background Information

The field of nuclear forensics has been a topic of intense discussion in scientific literature, public policy literature, and the popular press since 2003 (Harwood, 2012). Nuclear forensic science, also identified as "nuclear forensics," can be defined as a complete examination done on a nuclear and other radioactive material to identify the possible origin, intended use, and hazards related to the material, following its seizure from illicit trafficking or diversion (Harwood, 2012; John *et al.*, 2021). Following the detonation of a nuclear weapon, nuclear forensics examines interdicted nuclear materials and radioactive materials to detect signatures (elemental, isotopic, chemical, and physical) indicative of the materials' processing history and origin (Agency, 2015). The evidence or clues on the origin and intended use of nuclear or radioactive material will be acquired from the characteristic parameters gathered through nuclear forensic examination (Laili *et al.*, 2020). Nuclear forensic signatures are the combinations of characteristic parameters. To put it another way, signatures are the characteristics of a nuclear or other radioactive material that allow it to be distinguished from all other materials (Laili *et al.*, 2020). Uranium and its associated oxide species are among the most critical nuclear elements that require well-defined forensic signs (Schwerdt *et al.*, 2018).

Uranium is a naturally occurring radioactive element that has a significant impact on our daily lives (Balatsky & Severe, 2019). Uranium is used in both nuclear power plants and military weapon programs (Švedkauskaitė-Le Gore, 2008). Recent advancements in nuclear-grade uranium measurement, ore discoveries, and rising environmental challenges including storage and disposal have all been significantly impacted by uranium's specific role in these activities (Švedkauskaitė-Le Gore, 2008). Uranium is found in low concentrations (1–2 μg g^{-1}) throughout the earth's crust and is particularly abundant in mineral formations such as sandstone and quartz pebble conglomerate (Bradley *et al.*, 2020; Moody *et al.*, 2014). Low-grade uranium ore is a term used to describe mineral resources with a high uranium content of up to 2000 μg U g^{-1}. Uraninite ore can be found in rare circumstances (e.g., Canada) that contain up to 70% U by weight (Keegan *et al.*, 2012; Moody *et al.*, 2014). The majority of the world's uranium supply originates from low-grade uranium mineral resources that must be mined and concentrated (Bradley *et al.*, 2020). The fact that certain measurable parameters or signatures are specific depending on the geological source of the substance under investigation is taken into account by nuclear forensics. In a wide range of nuclear and other radioactive

materials all over the world, signatures like uranium isotope compositions as well as ratios, elemental impurities, Lead (Pb), Neodymium (Nd), rare earth elements (REE) patterns and Strontium (Sr) have been identified (John *et al.*, 2021).

Following a huge number of seizures involving plutonium and highly enriched uranium to smuggle nuclear material, the concept that certain features of a substance are inherent and may be utilized to determine the provenance of any recovered nuclear material emerged (John *et al.*, 2021; Khumalo & Mathuthu, 2018). In 1991, the first instances of nuclear smuggling were found in the Soviet Union, Italy, and Switzerland (John *et al.*, 2021; Khumalo & Mathuthu, 2018). More cases were discovered later in Germany, the Czech Republic, Hungary, and other central European countries (Aggarwal, 2016a; Khumalo & Mathuthu, 2018; Ntsohi, 2019). Nuclear materials that have been intercepted and smuggled could be converted as nuclear weapons (Asai & Limbeck, 2015).

Nuclear and other radioactive materials that are not regulated may pose a severe hazard to international society (Reading, 2016). To address these concerns, the International Atomic Energy Agency (IAEA)' office of nuclear security created a database to keep track of smuggling incidents (Reading, 2016; Vesterlund, 2019). The IAEA created the Incident and trafficking database (ITDB) in 1995 to record and analyse incidents in which nuclear and other radioactive materials were detected out of regulatory control (Ntsohi, 2019).

Between 1993 and early 2019, the IAEA ITDB recorded 3387 events involving nuclear or other radioactive materials that were not under regulatory control, and 759 of these events have been linked to criminal activities, with 16 of the criminal events (involving nuclear material) that may be used in nuclear weapons (highly enriched uranium or plutonium) (Vesterlund, 2019). These figures raised serious concern and require the development of rapid, reliable methods for determining the origin of nuclear or other radioactive materials discovered outside of regulatory control by nuclear laboratories (Ntsohi, 2019). Therefore, it is crucial to identify rare earth elements if this nuclear material is detected. Results from rare earth elements can be utilized as a nuclear attribution signature.

1.2 Problem statement

The theft and accidental loss of nuclear and radioactive materials, resulting in so-called material out of regulatory control (MORC) is a global issue of long-standing concern (Downes *et al.*, 2019). The improper handling, storage, or transport of nuclear or radioactive materials can lead to considerable long-lasting hazards as well as possible diversion and proliferation

(Moody *et al.*, 2014). While radioactive materials are usually kept under strict physical control and are constantly monitored, the possibility of malicious intent on the part of wrongdoers cannot be ruled out. It is important to detect their presence in different biological and environmental samples because these materials emit radiation and are hazardous to human health if they reach the human body even at extremely low levels (i.e. microgram amounts) (Harwood, 2012). Even though these undesirable practices are on the decline, nuclear terrorism is still considered the greatest danger due to its health risks (L'Annunziata, 2012).

Former US president, Barack Obama summarized the international community's consensus that "nuclear terrorism is one of the most challenging threats to international security" in his speech at the 2010 Nuclear Security Summit in Washington, D.C. (Kristo & Tumey, 2013). The terrorist attacks on September 11, 2001, in New York City and Washington DC, elevated the importance of nuclear forensics significantly, as policymakers became increasingly concerned about the prospect of well-organized terrorist organizations such as Al Qaeda, possessing a nuclear weapon or using a radiological dispersal device (RDD or "dirty bomb") (Harwood, 2012; L'Annunziata, 2012). By the end of 2016, the database had received 3068 reports, with 270 of them being documented cases of human trafficking or malicious use (Ntsohi, 2019).

Nuclear material trafficking cases have been reported to the South African Police Services (SAPS) in South Africa. Two containers of uranium materials (weighing 1.2 kg and 0.5 kg) were reported on 10th January 2012, and one container containing uranium was (weighing 0,8 kg) seized on 13th January 2012 both in the Sandton area, Johannesburg (Boshielo & Mogafe, 2015; Mogafe & Chakrov, 2015). Furthermore, two men were arrested on 14th November 2013 on suspicion of having uranium and some pills stored in a plastic bag (Mogafe & Chakrov, 2015). Lastly in Durban on 15th December 2015, it was reported that 1 kg of uranium-rich sample was seized by the South African Police Services (SAPS) (Melanofthalmidou *et al.*, 2015).

As a result, nuclear forensic science has emerged and nuclear materials have become a new discipline and part of forensic investigation (Ho, 2015). There has been very little study done on African nations in the area of nuclear forensics (Mathuthu & Khumalo, 2017). In Africa, there are uranium deposits in many countries (Mathuthu & Khumalo, 2017). Some nations, such as South Africa, Namibia, Zambia, and Tanzania, have actively mined uranium as a primary or secondary mineral (Dasnois, 2012). The IAEA Non-Proliferation Treaty, which aims to shield nuclear and other radioactive materials from unwanted monitoring, must be

adhered to by these nations (Ntsohi *et al.*, 2021). At the moment, no African country is known to have a National Nuclear Library (Ntsohi *et al.*, 2021).

These raised serious concerns and require the development of rapid, reliable methods for determining the origin of nuclear or other radioactive materials discovered outside of regulatory control (Ntsohi, 2019). If this nuclear material is intercepted, it is important to trace its origin and one key element that could assist in the determination of the origin is the rare-earth elements (REE) as a signature for nuclear material attribution.

1.3 Aim and objectives

1.3.1 Aim:

The aim of this project was to determine REE in uranium-bearing material for nuclear forensics purposes using ICP-MS.

1.3.2 Objectives:

The specific objectives of this study were to;

- separate and quantify REE present in uranium-bearing material.
- measure the concentration of REE in uranium-bearing material using ICP-MS.
- develop the REE pattern for use as a signature in identifying the possible origin of uranium-bearing material.

CHAPTER 2: LITERATURE REVIEW

2.1 Introduction

Nuclear forensics includes several branches of science and technology, such as radioanalytical chemistry, nuclear and radiochemistry, geochemistry, geology, nuclear and reactor physics, nuclear engineering and processing, material science, statistics, and more (Reading, 2016). Nuclear forensics is important in identifying the origin of any "lost" material and assists to strengthen the safeguards around it so that it can be put to effective use (Ho, 2015). Nuclear forensics has increased in importance as a tool in the fight against the expanding issue of illicit nuclear material trafficking, which currently poses a threat to international peace (Lina *et al.*, 2014). Due to the complexity of this type of investigation, a variety of analytical methods are used, such as radiometric measurements (using the gamma and alpha spectrometry), isotope ratio measurements (using thermal ionization mass spectrometry (TIMS) or inductively coupled plasma mass spectrometry (ICP-MS)), elemental analysis (using ICP-MS or laser induced breakdown spectroscopy (LIBS)), and structural analysis (using scanning electron microscopy (SEM) or infrared spectroscopy (IS)) (Varga *et al.*, 2011).

These measuring techniques could provide additional information on the material, each with various capabilities and limits. The front end of the nuclear fuel cycle product uranium ore concentrates (UOC), which is used in nuclear fuel, is frequently traded internationally. Through the processes of leaching and extracting, UOCs are produced from uranium ores. Their geographic and geological signatures, as well as their physical characteristics, chemical compositions, and impurity concentrations, are rather influenced by the nature of the raw uranium ores and the appropriate milling techniques (Badaut *et al.*, 2009). Therefore, it is possible to identify an unknown UOC by its elemental, anionic (Keegan *et al.*, 2012), and isotopic signatures (Varga *et al.*, 2011) and identify its origin (such as location, deposit, type of uranium ore, and milling procedures).

2.2 Radioactive decay

To attain the neutron to proton (N: Z) ratio of the closest feasible stable nuclide, an unstable nucleus must decay (Martin, 2012). There is typically a surge of energy that comes after this. Therefore, the sudden release of additional power from an unstable nucleus that results in the emission of particles or electromagnetic radiation can be characterized as radioactive decay (Ntsohi, 2019; Reading, 2016). In 1897, Ernest Rutherford revealed that there were multiple types of radiation, each with varying degrees of penetrating power (Ntsohi, 2019). He named

the less penetrating alpha (α) rays and the more penetrating beta (β) rays radiation emissions. It was discovered that a magnetic field could deflect rays and that the particles possessed a charge-to-mass ratio identical to the electron. Marie Curie discovered that particles were heavier particles after investigating their absorption qualities (Malley, 2011). With a larger magnetic field, Rutherford successfully deflected particles, and he and Royds eventually demonstrated that the particles were helium nuclei (Eichholz & Poston, 2018). Villard discovered a third sort of radiation, which he named gamma radiation. Gamma (γ) rays had no charge since they were not deflected by magnetic or electric fields, unlike α and β rays (Martin & Shaw, 2019).

2.2.1 Alpha (α) decay

Natural heavy nuclides with atomic numbers Z > 74 and synthetic transuranic elements with Z > 82 both experience alpha decay (the release of one alpha particle) (Bryan, 2018; Martin & Shaw, 2019). Physical variations in the parent isotope with atomic number Z and mass number A ($\frac{A}{Z}$X) lead to the production of a daughter isotope with atomic number Z-2 and mass A-4 ($\frac{A-4}{Z-2}Y$), which is the consequence of the spontaneous emission of a ^{4}He nucleus through two (2) protons and two (2) neutrons (Ntsohi, 2019; Walther & Wendt, 2020). The huge mass of the particle reduces the velocity to a percentage of the speed of light (c) despite the immense kinetic energy of the particle emission. Alpha particles are hence non-relativistic. Compared to other kinds of radioactive emissions, particles are easily halted by a sheet of paper and have a small range. Alpha particles are released with well-defined energies that are specific to the emitting nuclei, making spectroscopic measurements possible (Lilley, 2013). According to the equation 1 below, The daughter nuclide ^{237}Np is produced when the radionuclide americium-241 decays by alpha particle emission (Walther & Wendt, 2020).

$$\frac{241}{95}\text{Am} \rightarrow \frac{237}{93}\text{Np} + \frac{4}{2}\text{He} + 5.638\ \text{MeV} \qquad (1)$$

The americium nucleus loses two protons and two neutrons, resulting in a mass decrease of four and a charge reduction of two (Walther & Wendt, 2020).

2.2.2 Beta (β) decay

Similar to alpha decay, beta (β) decay occurs when the parent nucleus undergoes a physical change and becomes a new isotope (Reading, 2016). To become a more stable nucleus, an antineutrino ($\bar{\nu}$) or neutrino (ν) is produced by the unstable parent nucleus after one electron

(β^- decay) or a positron (β^+ decay) (Lilley, 2013; Ntsohi, 2019). Negatrons or negative beta particles are electrons that are released from the nucleus of a radioactive source that is decaying and has an imbalance between neutrons and protons (n/p) (Walther & Wendt, 2020). The n/p imbalance causes nuclear instability, which leads to the conversion of a neutron to a proton within the nucleus (Ntsohi, 2019; Walther & Wendt, 2020). Equation 2 shows the balanced charges which is maintained when an electron (negatron) is simultaneously created (Walther & Wendt, 2020).

$$\frac{1}{0}n \rightarrow \frac{1}{1}p + \frac{0}{-1}\beta + \bar{\upsilon} \quad (2)$$

where p denotes a proton, n stands for a neutron, and $\bar{\upsilon}$ denotes an antineutrino.

Energy of the released electrons ranges from Q-value to zero (Lilley, 2013; Martin, 2012). This is because $\bar{\upsilon}$ for the β^+ decay, the simultaneous emission of electrons and the conservation of the lepton number are required (Ntsohi, 2019). Under the category of β decay, there are two distinct types of radioactive decay modes: electron capture decay and β^+ decay. Both types cause a proton to turn into a neutron while maintaining the same atomic mass. While the capture of an atomic electron is referred to as electron capture decay, the emission of a positron is known as β^+ decay (Eichholz & Poston, 2018; Lilley, 2013; Martin, 2012). Both reactions produce a neutrino, which is released.

2.2.3 Gamma decay

Nuclei are frequently left in an excited state after the alpha and beta decay processes (Martin, 2012; Reading, 2016). When a nucleus enters a lower state, energy is lost. The transition energy (ΔE), which is the energy disparity between the starting and final states, can be carried by a γ photon (Ntsohi, 2019). Energy level transitions take place at specific energies and the γ rays that result from these transformations have well-defined energies (Lilley, 2013; Martin, 2012). Each photon emission has a different energy in the parent and daughter states as a result. The equation 3 illustrates the gamma decay of ^{238}U (Reading, 2016):

$$\frac{283}{92}U \rightarrow \frac{234}{90}Th + \frac{4}{2}He + \frac{0}{0}\gamma \quad (3)$$

In depopulating excited nuclear states, internal conversion (IC) competes with γ emission (Lilley, 2013; Moody *et al.*, 2014). An electron is de-excited by being ejected from one of the

atomic orbits when the external electromagnetic field of a nucleus relates with atomic electrons, transferring energy and angular momentum to an electron (Lilley, 2013). The electromagnetic force is responsible for both IC and γ decay.

2.2.4 Rates of radioactive decay

To achieve stability, radioactive elements undergo radioactive decay. Thus, radioactive decay is the spontaneous transition of unstable parent nuclei into more stable daughter nuclei until a stable daughter nucleus is attained. The decay constant (λ) is the likelihood of a given nucleus decaying radioactively per unit of time. The rate of decay for N radioactive nuclei in a sample is given by equation 4 below:

$$\frac{dN}{dt} = -\lambda N \qquad (4)$$

The negative sign denotes a reduction in the number of atoms (N) with time. We get the exponential law of radioactive decay illustrated in the equation 5 below by solving the differential equation above and imposing the boundary constraints $N = N_0$ at $t = 0$.

$$N_t = N_O e^{-\lambda t} \qquad (5)$$

The activity (A) of radioactivity is a measure of the number of disintegrations per unit of time. Radio-chemists discovered that the amount of radioactive atoms (N) in a certain generated sample containing one radionuclide was inversely correlated with the sample's activity (Eichholz & Poston, 2018; Lilley, 2013). Equation 6's representation of the fundamental law of radioactive decay explains this relationship (Lilley, 2013).

$$A = \lambda N \qquad (6)$$

Becquerel (Bq), or one disintegration per second, is used to measure the activity.
The activity can therefore be described as follows using the two equations (5 & 6) mentioned previously;

$$A = \lambda N_O e^{-\lambda t} \qquad (7)$$

Equation 8 is used to calculate how many atoms are present in a radioactive source.

$$N = \frac{M}{m} \times A_V \qquad (8)$$

where, M is the radionuclide's weight, m is its atomic mass, and A_v is its Avogadro's number of 6.02×10^{23} atoms per gram.

The average lifetime of the radioactive nucleus is the mean life τ of a radionuclide. Equation 3 is used in equation 9 to determine the number of nuclei that will decay between time t and time *t* + dt.

$$dN = \lambda N\, dt = \lambda N(0) e^{-\lambda t} dt \tag{9}$$

and

$$\tau = \frac{\int t dt}{\int dN} = \frac{1}{\lambda} \tag{10}$$

As stated in equation 11, the half-life $\tau_{\frac{1}{2}}$ can be expressed in terms of λ either τ or.

$$t_{\frac{1}{2}} = \frac{In2}{\lambda} = \tau In2 \tag{11}$$

Using equation 6 and equation 11, the activity can be expressed as shown in equation 12:

$$A = \lambda N = \frac{NIn2}{t_{\frac{1}{2}}} \tag{12}$$

The population of the daughter radionuclide is determined by the parent and daughter decay constants (Ntsohi, 2019; Reading, 2016). This is because the daughter population increases at the same rate as the parent population and then decays at its rate. When the parent's decay rate and half-life are much larger than the daughter's, the two will enter a condition of secular equilibrium (Ntsohi, 2019; Reading, 2016). The number of radionuclides created is equivalent to the pace at which they decay in this state; for example, ^{238}U has a much longer half-life of 4.47 billion years than its daughter ^{222}Rn (Ntsohi, 2019).

2.3 Nuclear fuel cycle

The nuclear fuel cycle is a dynamic system of processes that shows the pathway of nuclear fuel in several stages "before and after use within the reactor," and refers to chemical and metallurgical reactions that operate during these stages (Crossland, 2012). It is also used for the generation of electricity, as well as providing new fuel for nuclear reactors and managing the fuel once it has been used up. The main element in nuclear fuel nowadays is uranium (Mathuthu & Khumalo, 2017). The heavy radioactive element uranium is present in soil, seas, rocks, plants, animals, and people (Khumalo, 2017). A sequence of processes and operations is essential for uranium to be utilized as a fuel (Ntsohi, 2019). This cycle which begins with

ore mining and ends with the disposal of spent fuel and other types of radioactive waste, serves as an illustration of the origin of nuclear energy (Crossland, 2012). The nuclear fuel cycle is broken down into two stages: the front end, which consists of mining, milling, conversion, enrichment, and manufacturing; and the back end, which consists of temporary storage, reprocessing, recycling, and eventually waste disposal (Ntsohi, 2019). The descriptions of the various stages of the nuclear fuel cycle are illustrated in Figure. 2.1.

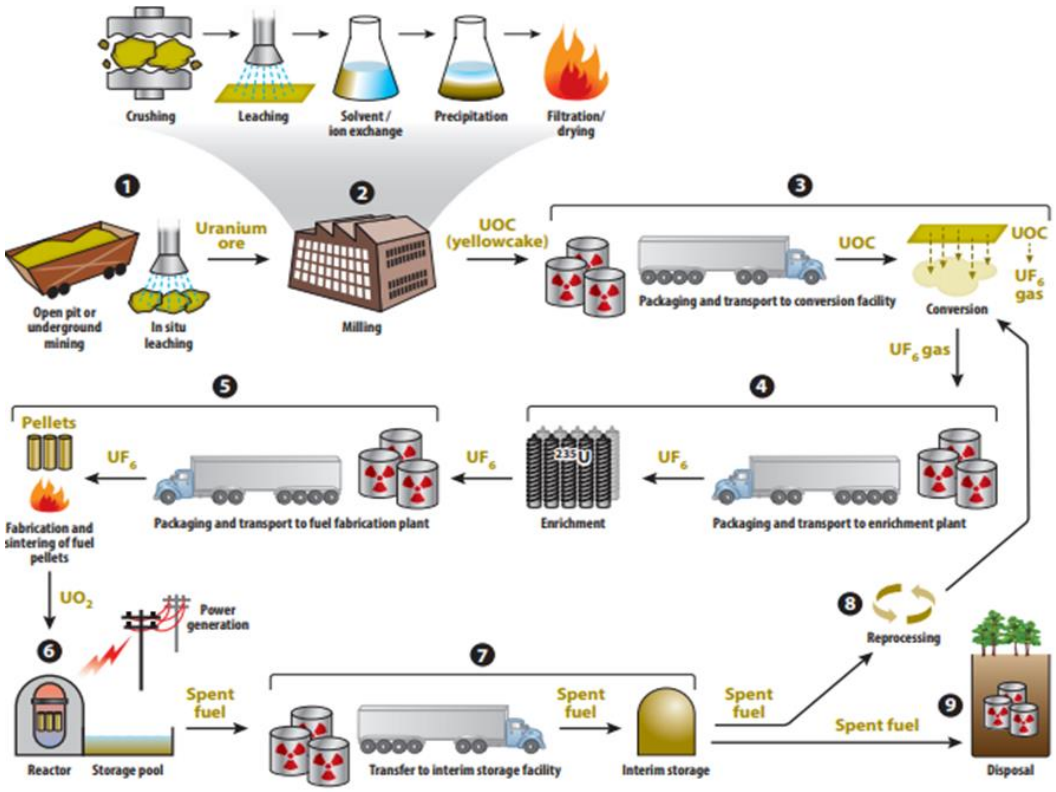

Figure 2. 1: Nuclear fuel cycle (Keegan *et al.*, 2016).

The following are the steps that make up the nuclear fuel cycle:

2.3.1 Uranium mining

Depending on the economy, geology, depth, and location of the deposit, uranium ore is extracted using one of three methods: open-pit mining, underground mining, or in-situ leaching mining (Khumalo, 2017; Reading, 2016). Mining methods have been changing. In 1990, 55% of world production came from underground mines, but by 1999 this had shrunk dramatically to 33%. From 2000, the number of new Canadian mines increased again, and with Olympic dam, it is now back to one-third (Crossland, 2012). In-situ leach (ISL or ISR) mining has been

steadily increasing its share of the total uranium production, mainly due to developments in Kazakhstan (Crossland, 2012).

Open-pit mining

Open pit mining shown in Figure 2.2 is used when the uranium deposits are near the surface usually less than 100 m deep. A hole is dug into the ground (topsoil and uneconomic rock) using large excavation equipment or explosives (Khumalo, 2017; Reading, 2016). Due to the ore's closeness to the surface, open pit miners dominated uranium mining till the past 50 years (Khumalo, 2017).

Figure 2. 2: One of biggest open-pit mining in Asia (Chen *et al.*, 2015).

Underground mining

Uranium reserves close to the surface were quickly depleted due to the high demand, and underground mining had to be used for deposits that were too deep for open cast (Ntsohi, 2019). Underground mining is called the conventional method as well as open-pit mining since they involve physical-mechanical work as opposed to non-conventional methods (Khumalo, 2017). Underground mining as shown in Figure 2.3, is commonly used where ore bodies are 100 m deeper, needing the construction of access shafts and tunnels but with less waste rock removed and less environmental damage (Crossland, 2012; Jarding, 2011).

Figure 2. 3: Underground mining (Freire & Cota, 2017).

In-situ leaching mining

When an aquifer in permeable rock that is enclosed in non-permeable rock has a uranium deposit, in-situ leaching is used (Ntsohi, 2019). A method of dissolving uranium in a porous ore body using oxygenated water or a leaching liquid (ammonium carbonate or sulphuric acid) and returning it to the surface for further refining is known as in-situ leaching as shown in Figure 2.4 below (Jarding, 2011; Khumalo, 2017; Reading, 2016). When compared to open cast and underground mining, this process is more cost-effective and produces less waste.

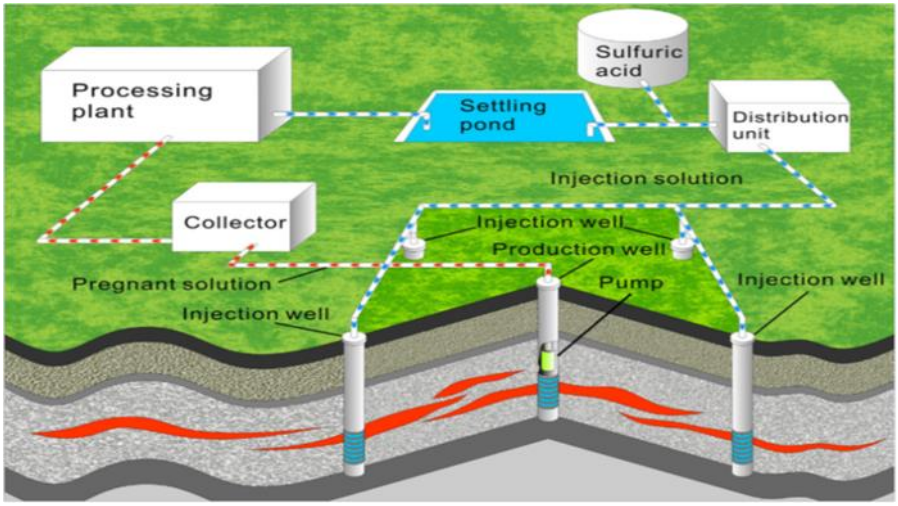

Figure 2. 4: *In-situ* leaching (Zhou *et al.*, 2020).

2.3.2 Milling process

If conventional mining has already been used, the uranium-bearing ore is first crushed in a dry process before being ground into the slurry inside a wet process (Piro & Lipkina, 2020). By increasing the material's surface area to volume ratio through crushing and grinding, chemical leaching is made easier (Piro & Lipkina, 2020). Crushing is a process in which ore rocks are sprayed with water and then crushed to a particle size of 200 mm in diameter by a large crusher (Ntsohi, 2019). There are two possibilities 15 cm of material is produced by initial crushing, and 1 cm by fine crushing. Semi-autogenous grinding or autogenous grinding is the most common method for crushing (Piro & Lipkina, 2020). Before leaching, to enhance surface area and hence boost the efficiency of the leaching process, all ores has to be ground (Reading, 2016). Roasting the material removes a significant number of organic materials, such as sulphides and carbon-bearing substances. Close to 668 °C, UO_3 is stable in the air but at higher temperatures, it decomposes to U_3O_8 (Piro & Lipkina, 2020).

The fine slurry is then created and leached in a solution, with the solution being chosen based on the ore materials (Piro & Lipkina, 2020). Acidic leaching needs particle sizes of less than 10 mm, whereas alkali leaching requires particle sizes of less than 0.5 mm (Reading 2016). To dissolve the uranium oxides, sulfuric acid (Piro & Lipkina, 2020) or an aqueous solution containing sodium bicarbonate and sodium carbonate (Ntsohi, 2019) are the most commonly used solutions (Piro & Lipkina, 2020). Figure 2.5 depicts a vehicle (A) transporting uranium ore to Key Lake Mill (B)

Figure 2. 5: Uranium ore slurry arrives (a) at the key Lake mill (b), Northern Saskatchewan, Canada (Erpenbeck, 2017).

Uranium recovery from a leached solution

Sulphuric acid (H_2SO_4) is used to finish acidic leaching, and oxidizing agents ($NaClO_3$, MnO_2, and Fe_2O_3) are needed if the uranium is tetravalent (Edwards & Oliver, 2000; Wilson & Krauskopf, 1997). Ferric iron serves as a catalyst in this process. The ideal leaching period is 12 hours at a temperature between 40 °C and 50 °C (Švedkauskaitė-Le Gore, 2008). When the ore feed contains a high carbonate content or other acid-consuming components, alkali leaching is necessary (Gupta & Singh, 2003). This process often uses Na_2CO_3, $NaHCO_3$, or CO_2 in the circuit. The development of a tricarbonate complex is what causes alkaline leaching, which is slower than acid leaching but more selective for the dissolution of uranium (Edwards & Oliver, 2000). The leaching is typically carried out in Pachucas, pneumatic agitation machines that circulate the pulp around the 15 m in diameter and 35 m height tank using compressed gas or steam (Gupta & Singh, 2003). When the pulp density is less than 50% solids, the use of Pachuca enables a high recovery of uranium within 20 hours when using acid leaching or 100 hours when using alkali leaching (Gupta & Singh, 2003).

Utilizing solid-liquid separation tools like filters, cyclones, or flocculants, the uranium-bearing solutions are separated from the leached solids and refractory components (Reading, 2016). A complex combination of cations, anions, and impurities can be found in the uranium solutions (Ntsohi, 2019; Reading, 2016). While acidic leach will contain significant levels of aluminum (Al), arsenic (As), iron (Fe), magnesium (Mg), molybdenum (Mo), nickel (Ni), titanium (Ti),

vanadium (V), zirconium (Zr), and rare earth elements (REE), alkaline leach has a high selectivity for uranium and produces a relatively pure solution (Švedkauskaitė-Le Gore, 2008; Wilson & Krauskopf, 1997). Further concentration and purification are needed because the leachate's uranium (U) concentration is still quite low (Reading, 2016). This is accomplished via the ELUEX method, ion exchange (IX) , or solvent extraction (SX). Undissolved particles that may be present in the solution are removed by filtration, decantation, sedimentation, or centrifugation (Nash & Lumetta, 2011).

Ion exchange

Ion exchange's main function is to concentrate and purify uranium-bearing material, usually through absorption or elution methods (Straub *et al.*, 2020). In order to create a pure and concentrated solution of U, it first entails the selective retention of U on anionic or cationic resins (Reading, 2016). According to (Hore-Lacy, 2016), uranyl bisulfate and uranyl trisulfate are the most frequently used liquors in acid processes (normal pH range: 1.5–2.5). Uranyl bicarbonate and uranyl tricarbonate are frequently utilized in alkaline liquors (typical pH of around 6 to 11) (Straub *et al.*, 2020). Most ion exchange processes employ a gel-type resin, which occupies a large portion of the sorption and elution columns. Some commercial gel resins used in uranium milling include Amberlite IRA-400, Dowex 21-K, and Permutit SK (Straub *et al.*, 2020).

Solvent extraction

This approach is frequently favoured when the solution's uranium concentration is high (e.g., 0.800 mg/L) (Straub *et al.*, 2020), but no efficient solvent extraction method has been discovered for carbonate solutions (Zhu & Cheng, 2011). Compounds are separated by solvent extraction according to how well they dissolve in two different immiscible liquids, where uranium ions are complexed into the organic phase (Reading, 2016). An aqueous solution's initial solubility of uranium is transferred to the organic phase (Straub *et al.*, 2020). This is accomplished by extracting the U(VI) from the strong nitric acid using solvents such organophosphate tributyl phosphate (TBP), which creates a uranium complex ($UO_2(TBP)2(NO_3)_2$) (Reading, 2016). The organic complex is then treated with weak nitric acid, which results in dissociation and the release of free TBP and uranyl nitrate (Reading, 2016). Then, by adding NH_3, the solution passes through another process where uranium-bearing compounds are precipitated, producing $(NH_4)2U_2O_7$ (Straub *et al.*, 2020).

Precipitation

The concentration of uranium in the solution is increased at the end of either the ion exchange or solvent extraction techniques (Straub *et al.*, 2020). The most challenging step in the milling and processing of uranium is the precipitation of uranium from the leach liquors (Straub *et al.*, 2020). Due to the U grade, gangue composition, and product specifications from the customer, each uranium mill has its own precipitant, drying, and operating conditions (Reading, 2016). Yellowcake is created during the precipitation process, which separates uranium-bearing compounds from the solution in the pregnant liquor (Straub *et al.*, 2020). This can be done by adding a neutralizing substance, such as hydrogen peroxide, ammonia, sodium hydroxide, or magnesia. The specific agent utilized depends on a number of variables, particularly the solution's composition, cost, and environmental factors (Straub *et al.*, 2020).

The process of moisture removal and drying at the end of precipitation varies depending on the processes that came before it, but it frequently requires rinsing with high-quality water (Reading, 2016). Uranium ore concentrate (UOC), often known as yellowcake, is the resulting powdered product. The UOC that is created at the end of the milling process might have varied forms depending on the chemical procedures used. This contains impurities such as triuranium octaoxide (U_3O_8), magnesium, sodium, or ammonium diuranate (such as $(NH_4)_2U_2O_7$). Yellowcake typically includes 20% to 25% combined oxygen and anionic chemicals, ranging from a few ppm to a few percent, and 65% to 75% uranium (Straub *et al.*, 2020). Depending on the method of precipitation and the temperature at which the precipitate was dried, UOC can be yellow, orange, brown, or dark green (Reading, 2016).

The yellowcake is subsequently delivered to a factory for conversion. Tailings are what is left over from the ore and contain harmful substances including heavy metals and long-lived radioactive elements in low concentrations (Khumalo, 2017). Despite having an 80% uranium concentration in yellowcake, uranium still requires additional processing before it can be utilized as reactor fuel. This is because the required uranium fuel should be purer and more consistent in composition (Ntsohi, 2019) . Thus, conversion is used to increase uranium purity.

2.3.3 Uranium conversion process

Uranium concentrate must be transformed into uranium hexafluoride (UF_6) in order to be used as fuel (Ntsohi, 2019), or a form for direct fuel fabrication for heavy-water reactors (i.e., UO_2, since heavy water reactors do not require enrichment). Typically, the sequence of operations is refined first followed by conversion (Murchie & Reid, 2020). All commercial enrichment

procedures worldwide utilize uranium hexafluoride (UF_6) as the feed material. The chemical's physicochemical characteristics make it the perfect substance for enrichment procedures (Murchie & Reid, 2020; Ntsohi, 2019). It contains unique triple point at 64 °C and 152 kPa, where small changes in temperature and pressure can be used to control the state of UF_6 as a gas, liquid, or solid (Murchie & Reid, 2020). Through a two-step process, the uranium ore concentrate is transformed into UF_6 (Khumalo, 2017).

In the initial stage, U_3O_8 is converted into uranium tetrafluoride (UF_4), a green salt with a melting point of 960 °C. The uranium concentrate is converted into by $UO_2(NO_3)_26H_2O$(UNH), dissolving it in acid, followed by purification and calcination to create UO_3 powder. The hydrofluorination of this powder using hydrofluoric acid causes it to become U_4 (Keegan *et al.*, 2016; Ntsohi, 2019). Through fluorination, UF_4 is changed into UF_6 in the second stage. These two phases can be carried out at distinct plants, as in the case of the hydrofluorination stage with the manufacture of UF_4, although they are typically carried out at the same plant (Nash & Lumetta, 2011). The conversion process can be done in two ways namely dry and wet process. The difference between the two processes is in the production of UF_6. In the dry process, UOC is converted directly to UF_6 to yield an impure form of UF_6 then Purification follows later on whereas with the wet process, UOC is purified first before fluorine gas is added (Khumalo, 2017).

2.3.4 Uranium enrichment process

Most thermal reactors need enriched uranium as fuel, which is done by the enrichment process, which raises the ^{235}U content to 3–5% by mass (Nash & Lumetta, 2011; Ntsohi, 2019). Natural uranium is made up of three isotopes: ^{238}U which has natural abundance of 99.28 %, ^{235}U,(0.711%), and ^{234}U, (0.0054%) (Nash & Lumetta, 2011). Remarkably,^{235}U is the fissile component that makes a nuclear reactor run, accounting for less than 1% of the total. The minute proportion of ^{234}U in uranium does not need to be addressed for our purposes, so we may focus on ^{235}U and ^{238}U (Collum, 2016). Uranium enrichment is the process of increasing the concentration of ^{235}U relative to the naturally occurring uranium (Khumalo, 2017). Two of the most common techniques for enrichment are gaseous diffusion and centrifugal enrichment (Silvennoinen, 2013). Due to its three main benefits: it is a gas at low temperatures, fluorine has just one isotope, and fluorine has a low atomic weight: both processes require UF6 as a feed material (Ntsohi, 2019; Silvennoinen, 2013).

Gaseous diffusion

The gaseous diffusion process was the first commercial, large-scale process. It was the first-generation enrichment technology, developed in the early 1940s during World War II (Murchie & Reid, 2020). The small mass difference between $^{235}UF_6$ and $^{238}UF_6$ allows for gaseous diffusion enrichment since the $^{235}UF_6$ travels relatively faster to a given temperature (Crossland, 2012). The average kinetic energy of gases in a mixture is the same in thermal equilibrium (Murchie & Reid, 2020). Each separation element in an enrichment facility is made up of a converter, also known as a diffuser. Diffusion barriers are contained in thousands of tubes in the converter. The technique is demonstrated in Figure 2.6 below. Submicron holes are perforated in the diffusion barrier or membrane (Murchie & Reid, 2020). The UF_6 gas is delivered into a diffuser unit with a porous membrane, and the gas is propelled through it by applying pressure across the membrane (Crossland, 2012; Murchie & Reid, 2020). Because the $^{235}UF_6$ molecules travel faster, they collide with the membrane more frequently and are thus more likely to pass through a pore (Crossland, 2012). As a result, the lighter isotope will be slightly enriched on the low-pressure (product) side, while the heavier isotope will be slightly depleted on the high-pressure (tails) side. The enrichment is captured via a continuous bleed on both the product and tail sides (Crossland, 2012).

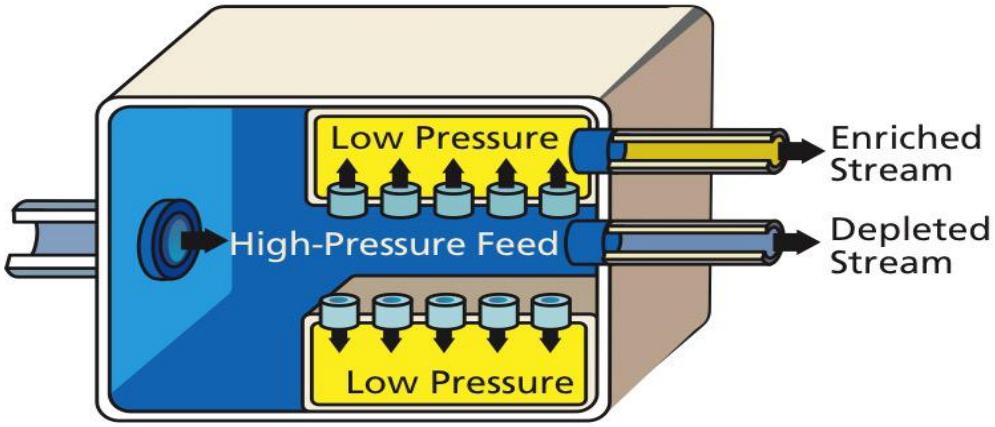

Figure 2. 6: Schematic representation of the gaseous diffusion process (Commission, 2020).

Gas centrifugation

A gas centrifuge is a long, narrow, vertical cylinder known as a rotor, which is rapidly rotated on its axis within an evacuated casing (Murchie & Reid, 2020). A schematic of a centrifuge, based on the Zippe design from the early 1960s (Murchie & Reid, 2020) is illustrated in Figure 2.7. UF_6 gas is introduced into a centrifuge with fast revolving tubes to enrich uranium in ^{235}U (Ko & Gao, 2012). The procedure involves feeding UF_6 gas into a centrifuge machine that is

spinning at an extremely high speed, with the centrifuge wall functioning as the rotor (Crossland, 2012; Murchie & Reid, 2020). The more massive molecules concentrate near the centrifuge walls, while the less massive molecules concentrate closer to the unit's central axis as a result of the acceleration caused by the rotation of the gas, which accelerates the gas molecules towards the direction of the centrifuge wall (Crossland, 2012; Ntsohi, 2019). A temperature gradient is then used to force the partially separated gas to spin along the centrifuge axis (Crossland, 2012). An enhanced product stream and a depleted tails stream are removed using "scoops" (Crossland, 2012; Murchie & Reid, 2020). The enriched UF_6 is subsequently transformed into UO_2, which is needed in the fuel fabrication process (Ntsohi, 2019).

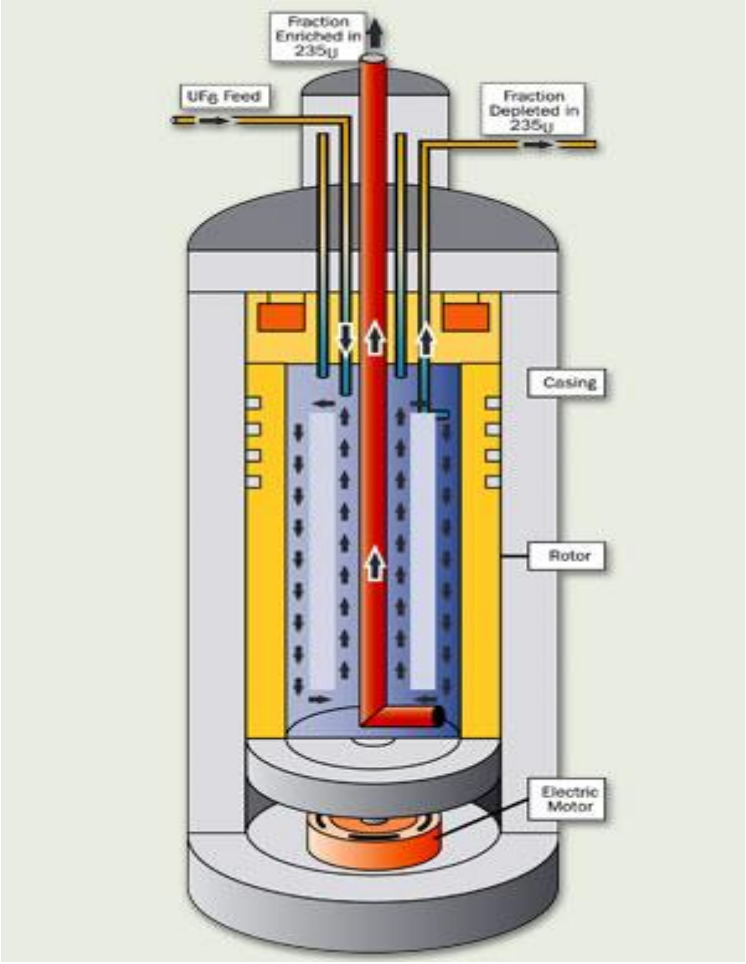

Figure 2. 7: Diagram of a gas centrifuge (Commission, 2020) .

2.3.5 Uranium fuel fabrication

The stage of enrichment involves converting UF_6 to UO_2, sintering UO_2 and ThO_2 into fuel pellets, encapsulating the fuel pellets into a fuel rod, and arranging the fuel rods to form a fuel assembly (Peiró & Méndez, 2013). This process creates nuclear fuel as an assembly with a certain shape and material type that is appropriate for the reactor design (Ntsohi, 2019). Fuel rods are cylindrical tubes that make up a fuel assembly. Uranium oxide pellets are encased in a zirconium alloy frame in these rods. Fuel rods are cylindrical tubes that make up a fuel assembly. Uranium oxide pellets are encased in a zirconium alloy frame in these rods (Park *et al.*, 2011).

The process of fabricating fuel includes the conversion of UF_6 to UO_2 powder, the creation of pellets, cladding, fuel rods, and finally assemblies (Ntsohi, 2019). The first phase in the fuel fabrication process is conversion. To convert UF_6 to UO_2 powder, a variety of dry and wet methods can be used (Chen *et al.*, 2012).The powder is pressed into small pellets, which are subsequently heated (or sintered) and machined to extremely tight tolerances (Collum, 2016; Ntsohi, 2019). The exact dimensions vary depending on the reactor type, but nuclear fuel pellets are typically 1 cm in diameter and a little longer (nuclear facility). Pellets are wrapped within one of the long thin rods, or pins, that characterize contemporary fuels after they have been machined and properly examined (Chen *et al.*, 2012; Collum, 2016; Ntsohi, 2019). Rods are produced and put into fuel assemblies, with the specific configuration varying depending on the type of reactor for which the fuel is intended (Collum, 2016). Figure 2.8 indicates Uranium fuel fabrication step by step process.

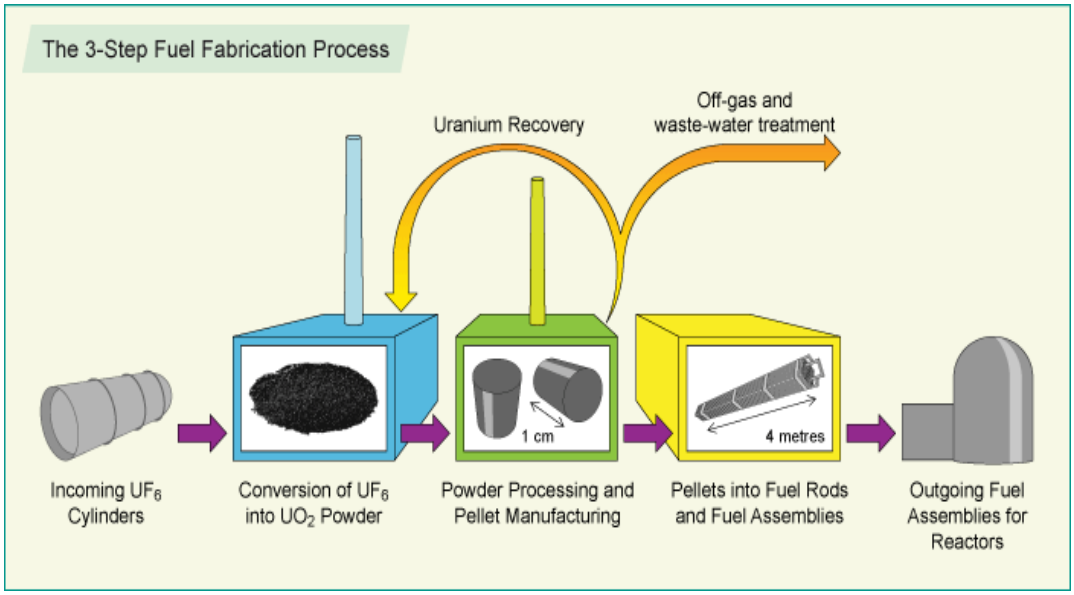

Figure 2. 8: Uranium fuel fabrication process (Agency, 2009).

2.4 Parameters that characterize uranium-bearing materials

Nuclear forensics is an important factor in the attribution process, requiring the analysis of nuclear material to identify forensic signatures based on established correlations between material character and process history (Kristo *et al.*, 2016; L'Annunziata, 2012). Although nuclear forensic science is a relatively new field, there is a substantial body of research on the topic that has been done and is still being done, with the main emphasis being on methodologies, usable measurement techniques, and the identification of parameters that can be used to determine the origin of a material (Ntsohi, 2019). Natural uranium signals are linked to either or both of the two categories; geological origin or process-relate (e.g., conversion of Ammonium diuranate to yellowcake**)**. This is similar to other nuclear forensics important materials like plutonium or HEU (Ho, 2015). Signatures are measurable parameters. Isotopic abundances, major, minor, and trace elements concentrations, as well as physical and chemical morphology are only a few examples of the "signature" features that must be present in illicitly recovered nuclear or other radioactive materials in order to identify a source or person (Reading, 2016). There is no single "signature" that can successfully identify a sample's origin (Kristo *et al.*, 2016; Ntsohi, 2019). Instead, a combination of the aforementioned is used to exclude origin possibilities rather than to determine a precise origin (Kristo *et al.*, 2016; Reading, 2016). Figure 2.9 depicts valid nuclear forensic signatures and how they might be used together to identify material to its source.

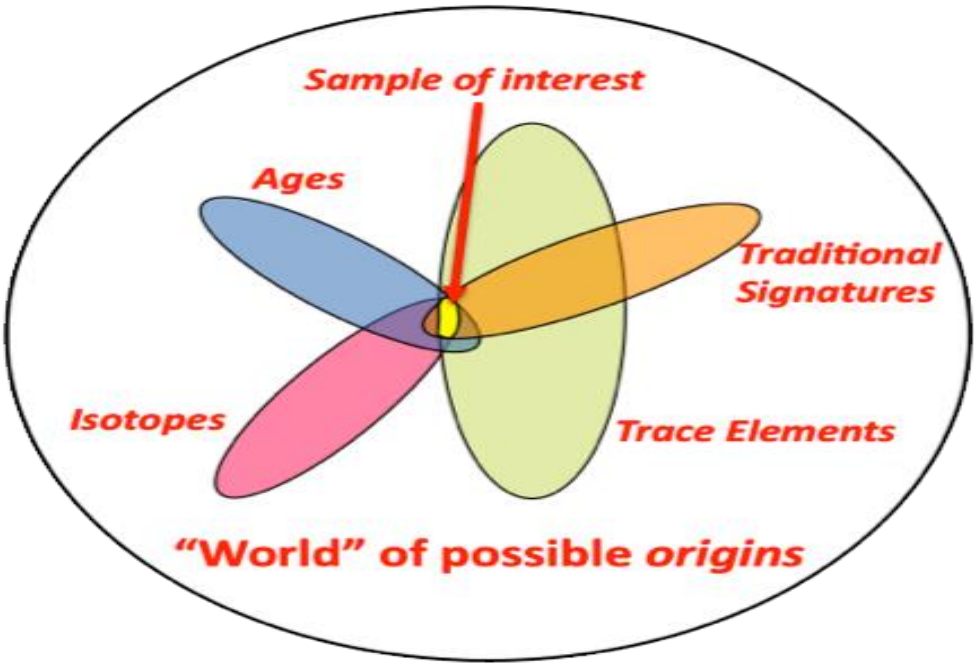

Figure 2. 9: Valid nuclear forensic signatures and the domain of possible material that fits such signatures are shown (Guenther *et al.*, 2013).

2.4.1 Patterns of isotopic composition in deposits

Uranium

The isotopic composition of uranium-bearing compounds is a crucial signature to obtain, and it varies substantially according to the provenance of the samples in the nuclear fuel cycle (Reading, 2016). The isotopes ^{234}U, ^{235}U, and ^{238}U are found in natural uranium (Ntsohi, 2019). Although the ^{235}U isotope abundance has been considered to be stable at around 0.71 percent, very precise ICP-MS measurements revealed that the $^{235}U/^{238}U$ ratio in nature is varied and can be attributed to natural isotope fractionation (Hiess *et al.*, 2012). For many years, the isotope ratio of $^{238}U/^{235}U$ was widely accepted as 137.88, and it was invariant until recently. Recent research has shown that this is not the case, since per-mil level variability in near-surface settings has been observed, resulting in a higher accuracy value of 137.797 for the average terrestrial composition (Reading, 2016).The terrestrial $^{235}U/^{238}U$ ratio varies by 1.3 percent in different geological materials, according to (Weyer *et al.*, 2008). (Brennecka *et al.*, 2010) discovered that the $^{238}U/^{235}U$ ratio ranges between 137.409 and 137.885. These studies' findings are based on tiny sample sizes and do not account for intra-mine variability. It would be necessary to use many isotope systems (like Pb and Sr) to determine the origin of an unidentified UOC, according to (Brennecka *et al.*, 2010). The existence of ^{236}U abundances in

higher proportions than those seen in natural uranium samples indicates that the uranium has been subjected to neutron irradiation and reprocessing (Ntsohi, 2019). In 2011, (Srncik, 2011) looked at the prospect of employing ^{236}U abundances in uranium ores as a global nuclear forensics signature and discovered substantial differences in the $^{236}U/^{238}U$ ratio for samples from Australia, Brazil, and Canada. Based on these findings, it was hypothesized that uranium isotopic ratios may be used as viable forensic signatures in ore samples (Srncik, 2011).

Lead

The lead (Pb) contains four stable isotopes: ^{204}Pb, ^{206}Pb, ^{207}Pb, as well as ^{208}Pb. The other three are generated from the decay of uranium and thorium radionuclides, with only ^{204}Pb being non-radiogenic (Ho, 2015). Natural lead has an isotopic composition of 1.4 percent (^{204}Pb), 24.1 percent (^{206}Pb), 22.1 percent (^{207}Pb), and 52.4 percent (^{208}Pb) (Ho, 2015). Two isotope ratios, $n(^{207}Pb)/n(^{206}Pb)$ and $n(^{208}Pb)/n(^{206}Pb)$, have demonstrated significant variation between mine sites and geological contexts because of the age of the deposit and the concentration of the associated parent U and Th (Keegan *et al.*, 2014; Reading, 2016).

(Varga *et al.*, 2009) noted that there is significant Pb variability in UOC from the same mine site due to heterogeneous Pb distribution in the ore body and processing effects from chemical separation and dilution with natural Pb. (Švedkauskaitė-Le Gore, 2008) demonstrated that samples from the same geographic location appear to have largely similar Pb isotopes (Ho, 2015; Ntsohi, 2019; Reading, 2016). Only one of the four stable lead isotopes is primordial; the other three, ^{206}Pb, ^{207}Pb, and ^{208}Pb, are by-products of the radioactive decay of ^{238}U, ^{235}U as well as the isotope ^{232}Th (Ntsohi, 2019). Thus, the stable isotope composition reveals both the age of the ore and the original U/Th ratio of the mine. Two considerations influence the choice of lead isotopes: First, the variety of geological processes that can be represented is increased by the creation of unique lead isotopes from ^{235}U and ^{238}U as well as thorium. Second, lead isotopes remain unaltered because they are stable in the geological context (Ntsohi, 2019). Because the ratio of lead isotope abundance at various manufacturing sites does not differ, the source of a significant divergence cannot be determined on its own. It must be supplemented with impurity data to resolve any impurity (Moody *et al.*, 2014).

Strontium

The validation of strontium isotopic composition as a nuclear forensic signal has also been studied. Variations in ^{87}Sr in nature result from the parent nuclide's extended half-life, which is ^{87}Rb (Reading, 2016). To identify the source of uranium ore concentrates, (Varga *et al.*, 2009) conducted research using the lead and strontium isotope ratio. They determined that lead and strontium isotope ratios were reliable techniques for determining the origin of uranium ore concentrate after finding variations in different mine samples (Varga *et al.*, 2009). A study by (Mayer *et al.*, 2013) was also undertaken. The study used an isotopic ratio of $^{87}Sr/^{86}Sr$. The isotope differences were found to range from 0.70785 to 0.76063, but there were instances of overlap between strontium isotopes from various mines (Ntsohi, 2019). As a result, the $^{87}Sr/^{86}Sr$ isotopic ratio of UOCs was evaluated for provenance (Ho, 2015; Mayer *et al.*, 2013; Ntsohi, 2019).

The studied UOCs' within-mine variability was significantly lower than that of the lead isotope ratios, indicating that this ratio was a more dependable indicator (less subject to manufacturing process effect) (Ho, 2015; Ntsohi, 2019). The ratios varied throughout a broad range of UOCs, making it possible to use them to differentiate between samples of various sources and to confirm the origin by comparing them to known samples (Ho, 2015). Both isotopic ratios have been utilized in the forensic analysis of UOCs from actual incidents (Varga *et al.*, 2011).

Sulphur

Due to the natural variability of $^{34}S/^{32}S$, studies were conducted to determine whether this was a valid signature. The use of the sulphur isotope ratio ($^{34}S/^{32}S$) to determine the origin of UOCs was recently published (Ho, 2015). In UOCs, there were clear changes in the sulphur isotopic composition of $\delta^{34}S$ ($\delta^{34}S$ takes into account values of $^{34}S/^{32}S$ of a standard) (Ho, 2015; Reading, 2016). A novel method for determining the $n(^{34}S)/n(^{32}S)$ ratio in uranium ore concentrate (yellowcake) samples was introduced in a prior study (Han *et al.*, 2013). Multi-collector inductively coupled plasma mass spectrometry (MC-ICP-MS) was then used to calculate the $^{34}S/^{32}S$ ratio. The approach was applied to actual UOC samples from various sources to test the applicability of the sulphur isotope ratio as a nuclear forensic signal (Krajkó *et al.*, 2016). Based on a combination of several leaching experiments and an assessment of the fluctuation in the sulfur isotope ratio throughout the manufacture of UOC from ore to U_3O_8 product in actual industrial samples, the study's findings indicated that process reagents have a considerable impact on the $n(^{34}S)/n(^{32}S)$ (Krajkó *et al.*, 2016).

Neodymium

Recently, the measurement and use of $^{143}Nd/^{144}Nd$ as a potential signature for uranium-carrying materials such as uranium ores and UOCs has been established (Ho, 2015). Using MC-ICP-MS, it was discovered that the $^{143}Nd/^{144}Nd$ isotope ratio significantly varied amongst UOCs, depending on the kind of geological deposit, the age of the deposit, and the Sm/Nd ratio (Krajkó *et al.*, 2014; Reading, 2016). Because many samples contain comparable Nd isotope ratios, even if intra-mine variability was noticeably less than that reported for Pb or Sr, it cannot be employed as a single signal for nuclear forensic investigation (Krajkó *et al.*, 2014).

Oxygen

In nuclear forensic research, oxygen isotopic ($^{18}O/^{16}O$) signatures may be useful for UOC samples (Ho, 2015; Ntsohi, 2019). (Pajo *et al.*, 2001) investigated the applicability of specific criteria, such as chosen impurities and $^{18}O/^{16}O$ ratios, for geo-location in nuclear forensic science in one of their works. In uranium oxide samples from different mines, small differences in $^{18}O/^{16}O$ isotope quantity ratios of less than 3% were discovered (Aggarwal, 2016a; Mayer *et al.*, 2013). Water is widely utilized as a solvent in uranium processing, variations in $^{18}O/^{16}O$ should be expected in the UO_2 output (Ho, 2015).

2.4.2 Impurities and trace elements

Rare earth element (REE) signature

The 15 lanthanides, as well as yttrium and scandium, make up the rare earth elements (REE), however, REE exclusively refers to the lanthanides (Zhuang *et al.*, 2017). These elements' chemistry is known to be very similar (Ho, 2015). REE (La - Lu) is one of the impurities that has been discovered to have greater discriminating power than others (Spano *et al.*, 2017). Since it reveals the mineralization process and the geological deposit, the REE concentration pattern in uranium ore and UOC serves as a critical signature for nuclear forensic investigations (Khumalo & Mathuthu, 2018; Reading, 2016). Throughout the nuclear cycle, REE maintains its chemical characteristics (Ntsohi, 2019). This indicates that a nuclear material generated from a single mine will have the same REE fingerprint as the ore, regardless of when it was produced in the nuclear cycle (Ntsohi, 2019). Additionally, since all REEs, with the exception of Ce (IV) and Eu, have the same oxidation state (3^+), there is no fractionation during the milling of uranium used to create UOC (II) (Reading, 2016). To eliminate the nuclear stability effect, the REE pattern is usually chondrite normalized (Reading, 2016).

Based on these discoveries and those from similar investigations, REE can be used as a useful signature to comprehend the process of uranium deposits and can be used as confirmation of uranium origin (Ntsohi, 2019). The REE concentrations were determined using HR-ICP-MS after chemical separation with TRU resin (Reading, 2016), and Recently, laser ablating doped cation exchange resin with reduced isobaric interferences from oxides and hydroxides (Donard *et al.*, 2015), as well as electron probe microanalysis (Keatley *et al.*, 2015), have been used. This study focused mainly on the rare earth elements (REE).

Anionic impurities

Numerous research has been conducted on the premise that anionic impurities can be utilized to signify the chemical process that material has gone through (Mayer *et al.*, 2013). Chemicals are used in the leaching, concentration, and purification of various ores. Common inorganic anions (F^-, Cl^-, NO^{3-}, SO_4^{2-}, and PO_4^{3-}) have been identified in uranium ore concentrations using ion chromatography. When the origin of seized nuclear material is determined, this technique may be used in nuclear forensic investigations (Ho, 2015; Keegan *et al.*, 2014). Fluorine levels were observed to be high in UOCs made from phosphate ores, which often contain apatite minerals ($Ca(PO_4)_3F$) (Reading, 2016).

In order to measure the anions present in samples of uranium ore concentrate Badaut *et al* developed a method. They used several sample techniques to examine changes both inside and between mines as part of their investigation (Badaut *et al.*, 2009). Although some changes were identified when utilizing alternative sampling methodologies, they were minor when compared to differences observed across samples from different mines, demonstrating that anion concentration patterns are legitimate nuclear forensic signatures (Kristo *et al.*, 2016; Mayer *et al.*, 2013).

Chemical impurities

Chemical impurities are elements that vary from the required impurities that are present during uranium processing (Aggarwal, 2016a). Impurities are derived from the raw materials used, others are pollutants introduced during the nuclear cycle, and some are purposely added to increase the material's efficiency (Aggarwal, 2016a). The impurity spectrum of a material can be used as a characterization parameter in both comparative and predictive studies (Peńkin *et al.*, 2016). By determining other non-radioactive impurity elements, (Keegan *et al.*, 2016) & (Aggarwal, 2016a) concluded that it is feasible to classify nuclear forensic signatures of the

origin or production process of components inherited from the body of the ore rather than through radioactive decay.

Metallic impurities

To enhance the end product and process nuclear material, impurities such as contaminants from feed or processing are added both consciously and unconsciously (Mayer *et al.*, 2013). As a result, the chemical makeup of nuclear material provides crucial details regarding the substance's properties. The elemental composition of individual particles in inhomogeneous samples like uranium oxide can be determined using analytical techniques like X-Ray Diffraction (XRD), X-Ray Fluorescence (XRF), Scanning Electron Microscopy (SEM) with dispersion X-ray spectroscopy (EDX), thermal analysis, or Fourier-Transform Infrared Spectrometry (FTIR) (Mayer *et al.*, 2013; Ntsohi, 2019). For the process of attribution, systematic research was undertaken on elemental fingerprints. Inductively coupled plasma-mass spectrometry (ICP-MS) was used in conjunction with statistical approaches such as analysis of variance (ANOVA), principal components analysis (PCA), and cluster analysis (CA) to determine the source of UF_6 samples (Kristo *et al.*, 2016) . It was later discovered that trace impurity analysis was a useful tool for characterizing materials and that, despite not always being unique, the impurity fingerprint was sufficient to distinguish between mines. In a comparable investigation, XRF, ICP-MS, and PCA were utilized (Kristo *et al.*, 2016). For analysis, (Keegan *et al.*, 2016) analysed and discovered the trace element composition of the UOC.

Organic impurities

The remaining organic molecules in uranium ore concentrate (UOC) from the milling process reveal information on the milling method and the solvents used (mostly for solvent extraction purification) (Ho, 2015; Reading, 2016). The diversity and abundance of several organic compounds were assessed in one study. By removing the UOC's organic components and quantifying them using Gas chromatography mass spectrometry (GC-MS), (Kennedy *et al.*, 2013) were able to distinguish between two separate UOC production lines. The organic fingerprints of the two production lines were considerably different, and the author thinks that this could be utilized as a nuclear forensics' identification technique.

2.4.3 Chronology of uranium (Age)

One of the most often used methods in nuclear forensic investigations is chronometry. When the material was last chemically separated or purified, an accurate age is obtained and the progeny isotopes are totally isolated from the radioactive parent (usually uranium or plutonium) (Ho, 2015; Reading, 2016). Analytical chemistry and radio-analytical chemistry are skills for measuring valuable nuclear signatures, and the age of the material (Keegan *et al.*, 2016). The knowledge that parents' nuclides decay into daughter nuclides is used in this parameter. As a built-in clock, the ratio of parent and daughter nuclides indicates the age of the material. This factor is crucial in determining the origin of the material since it can be used to rule out production or reprocessing facilities that weren't running or weren't processing the type of material at the time based on the production date (Ho, 2015; Ntsohi, 2019; Stanley *et al.*, 2013).

A "model" age is used to calculate the age of uranium or plutonium, and it is based on two key presumptions: Progeny radionuclides were completely separated from parent radionuclides at time zero, and the sample has been maintained as a closed system ever since purification/separation (i.e., no gain or loss of parent or daughter radionuclides other than radioactive decay) (Aggarwal, 2016a; Keegan *et al.*, 2016). Different parent-daughter nuclides, such as $^{234}U/^{230}Th$, $^{235}U/^{231}Pa$, and $^{236}U/^{232}Th$, can be used to create this predicted signature (Ho, 2015). The last parent-daughter pair only holds true for irradiated and reprocessed uranium, even if ^{236}U does not exist naturally. The investigation of $^{234}U/^{230}Th$ and $^{235}U/^{231}Pa$ requires a low detection limit of ^{230}Th and ^{231}Pa because of the lengthy half-lives of ^{234}U (2.46 x 105 years) and ^{235}U (7.04 × 108 years) and the slow in-growth of the daughter nuclides. Highly sensitive methods like inductively coupled plasma mass spectrometry are appropriate for such analysis (Varga *et al.*, 2012), It is necessary to use alpha spectrometry (AS) or thermal ionization mass spectrometry (TIMS) (Ho, 2015).

2.5 Analytical techniques in nuclear forensics

2.5.1 Gamma spectrometry

Gamma-ray spectrometry is one of the earliest analytical techniques that has been applied to dubious materials, which is the most appropriate, non-destructive means of characterizing illicitly obtained nuclear elements (Apostol & Maliuk, 2016; Reading, 2016). Gamma spectrometry, as shown in Figure 2.10 below, was one of the earliest nuclear forensic measurement techniques to determine the composition of a recovered nuclear specimen.

Gamma-ray spectrometry is utilized in a variety of areas, such as the monitoring of nuclear facilities, health physics, nuclear medicine, materials research, bioscience, environmental science, and industrial uses of radioisotopes. It is also employed in the field after a nuclear occurrence like an explosion (Auxier *et al.*, 2016; Khumalo, 2017). The estimated amount of uranium isotopes, the degree of daughter radionuclide in-growth in the typical decay series, and the presence of activation and fission products are all determined by gamma spectrometry. It is necessary to choose the detector appropriately for each sort of measurement (Apostol & Maliuk, 2016). For establishing the age of radioactive samples, the daughter/parent ratio as a function of decay time is commonly utilized. Age dating is difficult since the major isotopes (^{234}U, ^{235}U, and ^{238}U) have extremely long half-lives and only small amounts of daughter nuclides form during in-growth in the case of uranium (Bull & Smith, 2015) . In contrast, daughter nuclides have extremely short lifetimes relative to the lengthy half-lives of the parent isotopes, only a few decades. As a result, one may anticipate that the daughter nuclides will only be quantified by mass or alpha spectrometric methods following destructive chemical separation (Bull & Smith, 2015). The daughter/parent activity ratio for ^{214}Bi/^{234}U can, however, be determined by directly determining the count rates of the pertinent gamma peaks of ^{214}Bi and ^{234}U by low background gamma spectrometry (Bull & Smith, 2015; Reading, 2016).

Figure 2. 10: Gamma spectrometry HPGe well detector set up at CARST.

2.5.2. Mass spectrometry

In today's nuclear forensics examinations, mass spectrometry (MS) techniques are crucial (Stanley *et al.*, 2013). Mass spectrometry is used to assess the elemental and isotopic composition of nuclear materials because it offers incredibly high analytical precision and accuracy as well as the ability to identify both radioactive and stable isotopes (Harwood, 2012). With the aid of mass spectrometry, atoms or molecules are converted into positively or negatively charged ions, which are then divided based on their mass-to-charge ratio. The intensities of the resulting mass-separated ion beams are then measured (Harwood, 2012). These instruments are useful for comprehending a wide range of natural phenomena due to intrinsic qualities such as high sensitivity and application to all elements of the periodic table as well as big molecules such as proteins (Aggarwal, 2016b). At different stages of the nuclear fuel cycle, such as safety, nuclear material accounting, environmental monitoring, and nuclear forensics, mass spectrometry is becoming more and more crucial.

Mass spectrometry can quantify (often referred to as "assay") elements when used on a sample's major components by using an isotopic spike (isotopic dilution mass spectrometry) or by calibrating against reference solutions (in the case of solution-based methods like ICP-MS (Harwood, 2012; Stanley *et al.*, 2013). Future nuclear science and technology issues will need to be addressed using a range of mass spectrometric methods (Aggarwal, 2016b). Inductively coupled plasma source mass spectrometry (ICP-MS), glow discharge mass spectrometry (GDMS), thermal ionization mass spectrometry (TIMS), gas source electron impact ionization mass spectrometry (GS-EIMS), and secondary ion mass spectrometry (SIMS) are a few of the different mass spectrometric techniques (Aggarwal, 2016b). The following section discusses a number of mass spectrometry methods.

Thermal ionization mass spectrometry (TIMS)

Thermal ionisation mass spectroscopy (TIMS) is a single-element analytical technique that necessitates the presence of the sample in its purest form (Jariwala, 2014). TIMS has been used for decades and is well suited for extremely sensitive and precise measurements of isotope ratios, with an overall detection efficiency of 0.1 percent and accuracy values of even better than 0.01 percent (Kristo, 2020; Walther & Wendt, 2020). Typically, sector-field mass spectrometers with acceleration voltages of 3 to 10 kV are used (Walther & Wendt, 2020). Figure 2.11 shows small amounts of highly pure analytes which are deposited onto a clean metal filament, which is commonly constructed of rhenium or tungsten, in TIMS (Aggarwal, 2016b; Stanley *et al.*, 2013). The sample is then heated by sending a current through the filament in the vacuum of the ion source; average temperatures attained range from 1,000 °C

to 2,500 °C (Stanley *et al.*, 2013). If an element's ionization potential is low enough in comparison to the filament's work function, a fraction of its atoms are ionized by interaction with the filament surface at high temperatures (Kristo, 2020). The Saha-Langmuir equation, which includes an exponential of the difference between the filament material's work function (symbol) and the element's ionization potential (I), is the basis for the formation of positive ions in TIMS. The filament material should have a high melting point in addition to a high electronic work function (Aggarwal, 2016b). Equation 13 describes the proportion of positive ions to neutrals in thermal equilibrium.

$$\frac{n_+}{n_0} \propto e^{\frac{(\Phi - I_p}{kT}} \qquad (13)$$

For TIMS analysis of elements of interest in nuclear science and technology, positive atomic or molecular ions are typically used (Aggarwal, 2016b). Chemical separation methods and ionization temperature can both improve the TIMS analysis' specificity (Kristo, 2020). Two of the most important disadvantages of TIMS are the required time-consuming sample preparation (such as separations and filament preparation) and very poor analyte ionization, independent of sample loading method (Jariwala, 2014; Stanley *et al.*, 2013). As a result, some interest in using multi-collector MC-ICP-MS technique in current nuclear forensics research has grown (Stanley *et al.*, 2013).

Figure 2. 11: Thermal ionization at a sector-field mass spectrometry (Walther & Wendt, 2020).

Inductively coupled plasma mass spectrometry (ICP-MS)

In the past, many processes were needed to get the impurity spectrum of materials based on uranium. Although sufficient at the time, these methods lacked sensitivity, required a lot of time, and occasionally caused matrix and spectral interferences that made it difficult to directly identify contaminants (Ntsohi, 2019). As a result, MC-ICP-MS, as shown in Figure 2.12, was adopted into nuclear laboratories all around the world, allowing for accurate measurements of several samples. ICP-MS is a precise analytical technique that measures the mass-to-charge ratio of an ionized sample to determine its elemental and isotopic composition (Swinney, 2015). However, spectrometry equipment is pricey to own (costing between $200,000 and $500,000), as it necessitates a room that is reasonably large and a technician with the necessary training (Mathuthu *et al.*, 2017). Additionally, mass spectrometer techniques are destructive, but gamma spectrometer techniques are straightforward, non-destructive, and allow for the measurement of isotope radio activity, which can then be used to infer isotopic composition (Khumalo, 2017).

In MC-ICP-MS, purified sample solutions are inhaled into a plasma after being directly disseminated in a spray chamber (Stanley *et al.*, 2013; Walther & Wendt, 2020). The sample solution dissociates and the analyte effectively ionizes due to the plasma's high temperature (Kristo, 2020). Ions are subsequently sent into a mass spectrometer, where mass discrimination is usually accomplished via a double-focusing technique. Ions of various masses are simultaneously detected by a bank of detectors that are identical to those used in TIMS (Stanley *et al.*, 2013). With detection limits ranging from 0.1 parts per billion (ppb) to a few tens of ppb, ICP-MS is excellent for precisely measuring trace elements in solutions. ICP-MS measurements of some elements, such as Carbon (C), Oxygen (O), and Sulfur (S), are challenging because of background, interferences, or inefficient ionization(Kristo, 2020; L'Annunziata, 2012; Walther & Wendt, 2020).

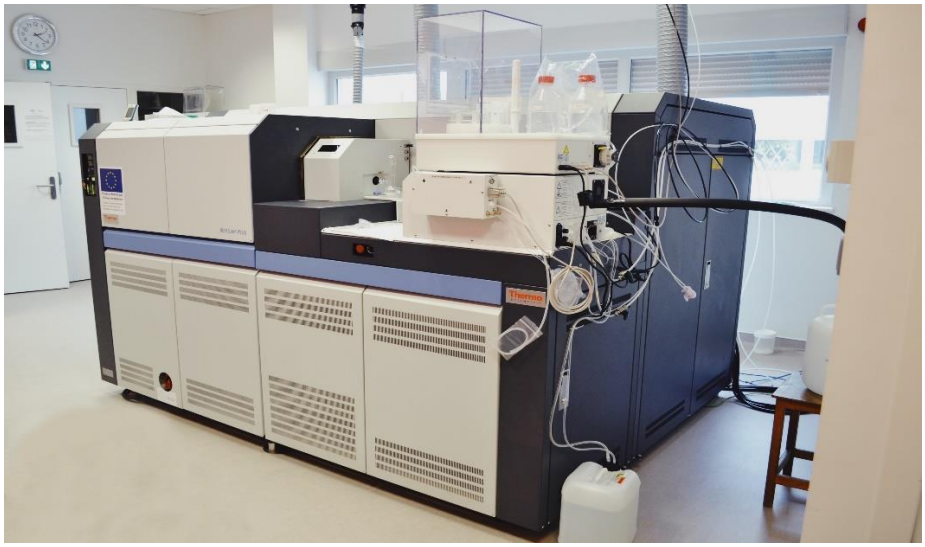

Figure 2. 12: Multi-collector - inductively coupled plasma mass spectrometry (MC-ICP-MS) (Walther & Wendt, 2020).

Secondary ion mass spectrometry (SIMS)

Using depth profiling and mapping of elemental and isotopic distributions, secondary ion mass spectrometry (SIMS) is a high-sensitivity surface imaging technology used to analyze mono and multielement traces in solid materials or thin layers (Walther & Wendt, 2020). SIMS (Figure 2.13) can be used to characterize bulk materials with detection limits as low as a few parts per billion (Kristo, 2020). SIMS relies on a concentrated beam of primary ions (Ar^+, Ga^+, Cs^+, $O2^+$, O^-) bombarding solid materials to produce ions (Stanley *et al.*, 2013). The secondary ions are sent into the MS instrument for examination after being sputtered. These ions are the result of primary ions transferring kinetic energy into the solid substance to a particular depth (Kristo, 2020; Stanley *et al.*, 2013). The yield of secondary ions for a given element is determined by its ionization potential as well as the specimen's physicochemical parameters, such as thickness, chemical makeup, and even surface quality (Stanley *et al.*, 2013; Walther & Wendt, 2020). Because of this, SIMS efficiency is extremely dependent on element and sample makeup, making it challenging to get absolute concentrations (Kristo, 2020). Utilizing relative quantities like isotope ratios or depth profiling of trace elements using relative abundances, SIMS is mostly used for element imaging (Walther & Wendt, 2020).

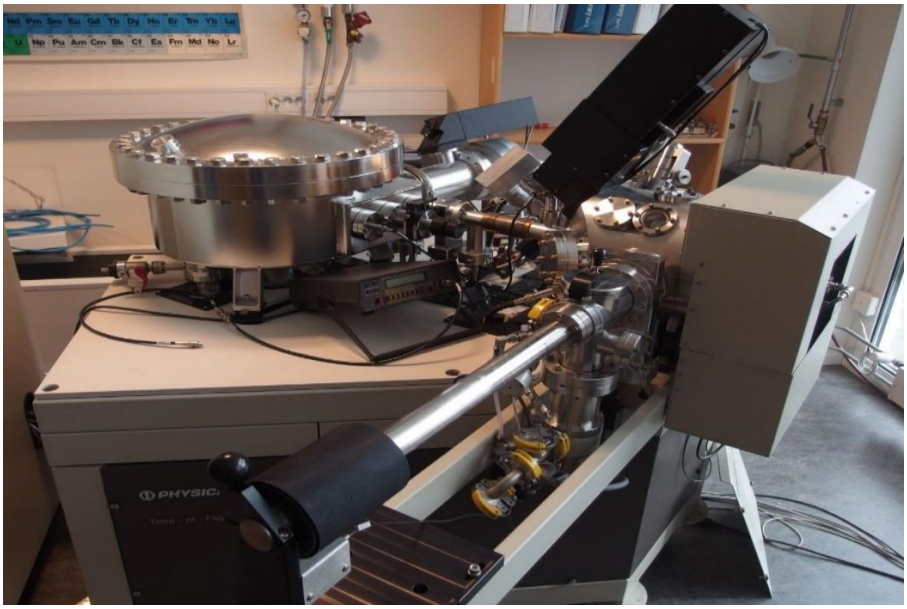

Figure 2. 13: Secondary ion mass spectrometry equipment (Walther & Wendt, 2020).

2.5.3. Alpha spectroscopy

Alpha spectrometry is a widely used radio-analytical technique. It focuses on the emission of particles (such as helium nuclei) to detect radionuclides, is frequently used in nuclear forensics investigations (Stanley *et al.*, 2013). Helium detectors such as liquid scintillation counters, gas ionization detectors, and ion-implanted silicon semiconductor detectors can all be used to measure particles (Kristo, 2020; Vajda & Kim, 2011). Silicon semiconductor detectors are the most widely utilized. Figure 2.14 represents a simple alpha spectrometer system (Stanley *et al.*, 2013). Compared to other radiometric techniques like X-ray spectrometry, alpha spectroscopy has a very low background due to the small range of a-particles and does not experience detector efficacy changes with energy (4 MeV to 9 MeV) (Aggarwal, 2016c; Kristo, 2020). Without the aid of a calibration standard for efficiency, alpha activity ratios can be precisely calculated without regard to the dependence of efficiency on energy (i.e., intrinsic efficiency of one) (Aggarwal, 2016c). Additionally, compared to other mass spectrometry methods like thermal ionization mass spectrometry (TIMS), inductively coupled plasma source mass spectrometry (ICP-MS), and others, the instrumentation is less expensive (Aggarwal, 2016c).

Numerous benefits of alpha spectrometry include inexpensive equipment costs, minimal background noise, excellent selectivity, and multi-chamber systems' high throughput capabilities (Stanley *et al.*, 2013; Walther & Wendt, 2020). Alpha spectrometry is particularly helpful as an addition to MS methods to account for short-lived nuclides (for example, species

with t1/2100) (Stanley *et al.*, 2013). The major downside of alpha spectrometry is that bulk matrix, compounds that interfere with the recovery of the element of interest, and other alpha emitters are typically removed using time-consuming chemical separation methods (Kristo, 2020; Walther & Wendt, 2020). Only a few specific applications allow for alpha spectrometry without chemical separation (such as the determination of airborne concentrations of radon progeny) (Kristo, 2020; Walther & Wendt, 2020).

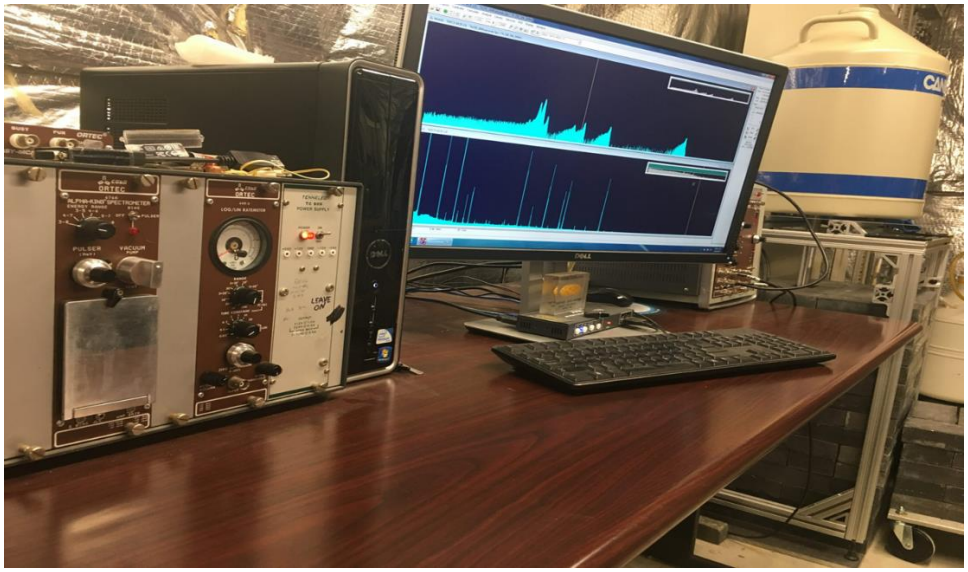

Figure 2. 14: Alpha particle spectrometry (Stanley *et al.*, 2013).

2.5.4. Scanning electron microscopy

In nuclear forensic investigations, the scanning electron microscope (SEM) is a crucial tool and the most popular way to examine the microstructure and morphology of materials. Direct comparisons between a previously identified UOC and an unknown sample were performed using SEM (Figure 2.15) (Keegan *et al.*, 2014). The morphology of nuclear material is studied using SEM (Jariwala, 2014). Nuclear materials' morphologies can disclose details about their processing history, and morphologic features can be utilized in nuclear forensic analysis with other data, such as elemental characterization (Tamasi *et al.*, 2016). At extremely high magnifications of up to 500 000x, SEM can produce images of an object's surface with resolution on the order of nanometers (Kristo, 2020; Stanley *et al.*, 2013). This method includes scanning a focused beam of strong electrons over the sample in order to detect backscattered or released electrons from the sample surface. Images are produced using the flux of electrons

from the sample surface as a function of the electron beam scanning location. Understanding how the object was made and identifying materials from various origins may benefit from knowing this knowledge (Kristo, 2020; Stanley *et al.*, 2013). Although SEM is a relatively simple method to utilize, sample preparation processes can have an impact on image quality (Stanley *et al.*, 2013). Samples are constrained in size by the SEM chamber's dimensions, which are typically in the range of inches, must be able to survive vacuum in the SEM chamber, and may need pre-treatment (for example, conductive coating) (Kristo, 2020; Stanley *et al.*, 2013).

Figure 2. 15: Scanning electron microscopy (Keegan *et al.*, 2014).

CHAPTER 3: METHODOLOGY

3.1 Introduction

The basis of the verification measurements in the framework of nuclear forensics is the measurement of nuclear material, which provides a clue for determining the origin of samples. The necessity to adopt safety and security measures to prevent and manage the unauthorized use of nuclear and other radioactive materials has been prompted by the growing interest in uranium mining in Africa. One such measure is the use of nuclear forensic techniques to establish a national nuclear library. ICP-MS technique was used to conduct the analysis required for the study. The samples being studied were taken from Witwatersrand region of South Africa shown in Figure 3.1. With over 52,000 tonnes (1,672 Moz.) of gold produced there to date, more than a third of all gold ever produced on earth, the Witwatersrand basin is the largest goldfield in the world. An estimated 30,000 tonnes (965 Moz.) of inferred resource are present in the basin (Tucker *et al.*, 2016). The Orange Grove quartzite, a white quartzite ridge, is the basin's lowest geological stratum. The Northern scarp edge of the Witwatersrand plateau in the Johannesburg area is formed by this notable structure (Tucker *et al.*, 2016).

The study area is a gold mining location located about 70 kilometres west of Johannesburg in Gauteng province in South Africa (Kamunda *et al.*, 2016a; Nwaila *et al.*, 2021). It is located between the latitudes 26″18’S–26″26’S and the longitudes 27″23’E–27″31’E. Exploration for gold began in the area in 1898, and mining began in 1945 (Kamunda *et al.*, 2016b). The area, which is roughly 86 km^2 in size, is located in the lower middle part of the Wonderfonteinspruit catchment area (WCA), in the West Wits line (Far West Rand) Goldfield. Deep-level (500–4000 m), high-grade underground mining as well as low-grade, surface rock dump mining are both used in mining (Kamunda *et al.*, 2016b).

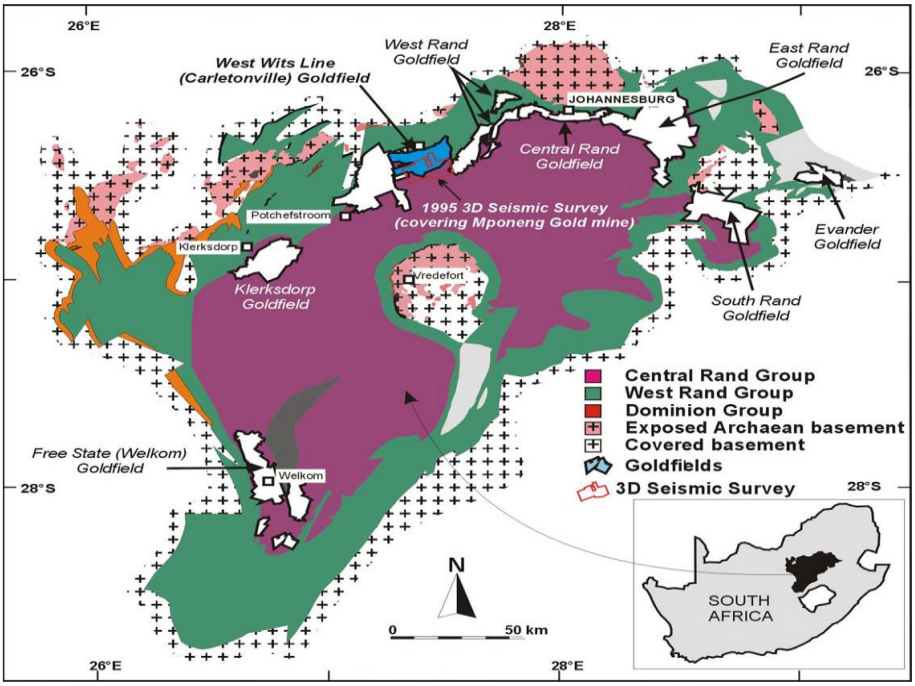

Figure 3. 1: The location map of the West Wits line (carletonville) goldfields of the Witwatersrand basin in South Africa (Manzi *et al.*, 2015).

3.2 Sample collection

Two (2) samples of uranium ore and four (4) uranium ore concentrate samples were obtained at the Carletonville mining site (Witwatersrand basin). An important step in the analytical process is sample preparation. Because the ICP-MS analytical technique requires that samples be introduced in liquid or aerosol form, samples must be homogenous before analysis for greater precision and accuracy. All of the samples were transported to the North-West University, Centre for Applied Radiation and Technology (CARST) to ensure uniformity. The samples were prepared and evaluated at the CARST laboratory.

3.3 Methodology of ICP-MS

3.3.1 ICP-MS technique

In the past, obtaining the impurity spectrum of uranium-based materials required different procedures. These processes were sufficient at the time, but they lacked sensitivity, demanded a lot of time, and prevented direct impurity assessment (Ntsohi, 2019). The recommended analytical method is ICP-MS, as illustrated in Figure 3.2, which has the ability to perform multi-element analyses and has a high sensitivity with a detection limit of ppt-ppq (Bazilio & Weinrich, 2012).

Figure 3. 2: Perkin-Elmer NEXION 2000 inductively coupled plasma-mass spectroscopy instrument at CARST.

The quadrupole ion deflector and dual mode detector are features of the NexION 2000 ICP-MS (Figure 3.4) in page 43. ICP-MS is a strong analytical technique that measures the mass-to-charge ratio of an ionized sample to determine its elemental and isotopic composition (Swinney, 2015). The method combines ICP's effective ion production features with MS's skills to provide a wide range of capabilities. Only a few of these characteristics include high precision (1% uncertainty), increased detection limits (parts per billion (ppb), higher throughput, the ability to handle both simple and complex matrices, enhanced detection capability, and the potential to extract isotopic information (Kristo, 2011). However, there are certain disadvantages to using this method. It is pricey, and it necessitates significant sample preparation.

3.3.2 ICP-MS instrumentation

The ICP-MS system can measure the coloured elements in Figure 3.3 quantitatively and provide a total amount of the individual elements of interest (Al-Hakkani, 2019). In addition to being more thorough and taking place in a chemically inert environment, plasma ionization has a number of advantages over conventional ionization techniques like flame ionization. Additionally, the temperature profile of the torch is comparatively uniform, minimizing the consequences of self-absorption. For ionization processes, curves for linear calibration have

been recorded spanning multiple orders of magnitude. The mechanisms that allow ICP-MS analysis to take place is described in greater depth.

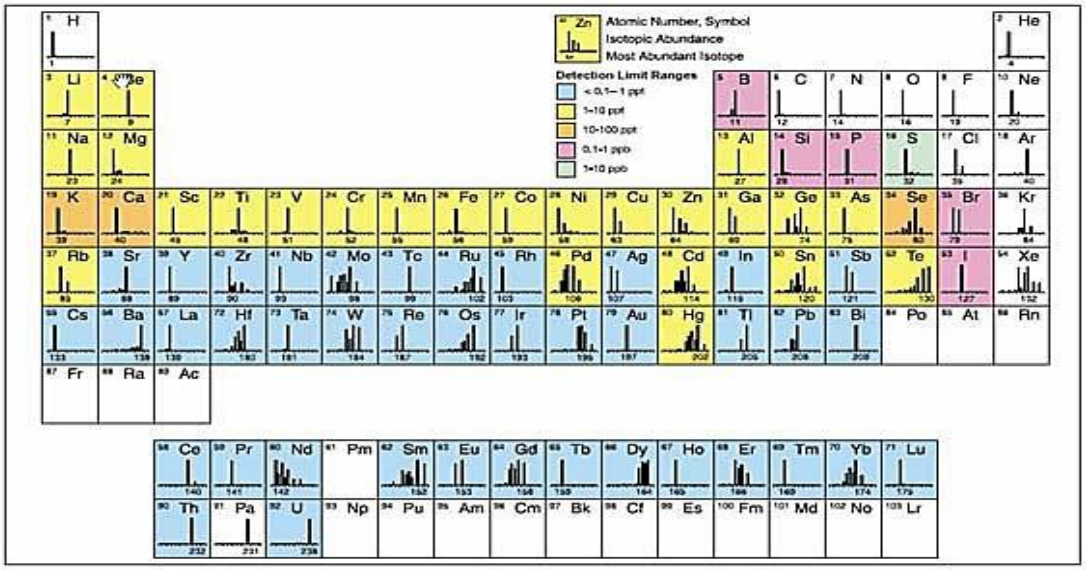

Figure 3. 3: Elements detectable by ICP-MS analysis (Perkin-Elmer) (Al-Hakkani, 2019).

Sample introduction

A sample can be introduced in a variety of ways, and the method used is determined by the sample's physical features. Although each approach is essentially different, they all aim to sweep the sample of interest into the ICP flame in a gaseous or aerosol form for analysis (Bazilio & Weinrich, 2012). The nebulizer and spray chamber are the most important parts of the sample introduction system. A sample is introduced into the system as an aerosol by aspirating a liquid sample or a dissolved solid sample into a nebulizer (as was the case in this study) or by laser ablation to convert a solid sample directly into an aerosol. Using a peristaltic pump, the liquid sample is transferred from a vial into the nebulizer (Ntsohi, 2019). As liquid droplets form on the needle, argon gas is nebulized by a second needle that runs parallel to the sample needle. The spray chamber then selects incredibly small droplets (m) from the aerosol to inject into the plasma (Bazilio & Weinrich, 2012; Borg & Hutcheon, 2013).

ICP torch

In the ICP torch, a concentric quartz lattice is wound around a copper induction coil. The RF coil is powered by an oscillating radio-frequency (RF) generator, and argon gas is continually pumped through the quartz torch (Bazilio & Weinrich, 2012). Plasma (a gaseous mixture that is electrically conducting) is produced when argon gas is seeded with a spark from a Tesla device. The spark ionizes some argon, and the resulting cations and electrons rush in the direction of the RF coil (Bazilio & Weinrich, 2012). High temperatures result from the collision of the cations and electrons with other argon molecules during this acceleration. If enough argon is supplied, the plasma will attain equilibrium and maintain a temperature of approximately 6,000°C throughout the investigation (Al-Hakkani, 2019). The nebulized aerosol enters this high-temperature plasma, where it is dried to a solid before being heated to a gas, a process known as atomization (Borg & Hutcheon, 2013; Ntsohi, 2019). Until these atoms release an electron and ionize, or become ionized, they will continue to receive energy from the plasma. The new ions then leave the torch and reach the interface (Bazilio & Weinrich, 2012).

Interface

In general, the interface is the point when a sample from the ICP section of the instrument is introduced into the mass spectrometry (MS) (Bazilio & Weinrich, 2012). The instrument's interface allows the ICP and MS sections to be connected (Al-Hakkani, 2019). The sampler cone is the first component the sample matrix encounters following ionization in the ICP torch (Ntsohi, 2019). A water-cooled cone has a tiny aperture here that lets hot plasma gas into a depressurizing chamber. In this chamber, the gas expands quickly due to rapid cooling. A portion of this gas is then pumped into a chamber that maintains the same vacuum as the MS after passing through a skimmer cone. This two-step pressure drop allows the ionic gas to reach the MS at the proper temperature and pressure (Bazilio & Weinrich, 2012).

Single ion lenses focus the ion stream into the quadrupole area after it passes through the sample and skimmer cones. Plasma ionization produces nearly all positively charged ions, which repel each other. The ions are guided through a charged metallic cylinder that prevents the ion beam from diverging. A dynamic reaction cell is included in the Elan DRC-e ICP-MS (DRC) (Bazilio & Weinrich, 2012). The Dynamic reaction cell (DRC) is situated between the lens and the quadruple in the vacuum chamber. When using the DRC mode, the ion beam is

chemically modified to eliminate interferences. The user controls the type of reaction gas and pressure in the computer software (Bazilio & Weinrich, 2012). Interference is avoided by disrupting the chain of events that would otherwise result in it. When the DRC mode is disabled, the DRC is a multipole device that transmits ions to the MS analyser chamber (Al-Hakkani, 2019). The elemental composition of matter samples, the structures of inorganic, organic, and biological molecules, the qualitative and quantitative composition of complex mixtures, the structure and composition of solid surfaces, and the isotopic ratios of atoms in samples are all investigated using mass spectrometry. When energetic electrons hit analyte molecules, enough energy is transferred to the molecules, causing them to become excited. Relaxation happens when a portion of the molecular ions are fragmented to generate ions with lower masses. The mass-to-charge ratio (m/z) of ions is used to disperse them in the mass analyzer (Al-Hakkani, 2019; Bazilio & Weinrich, 2012). After then, a computer interface is used to collect and save data from all populations. All of the components of a mass spectrometer, aside from the signal processor and readout, must operate at low pressures (Bazilio & Weinrich, 2012). Figure 3.4 shows stages that make up a process of ICP-MS system (Bazilio & Weinrich, 2012).

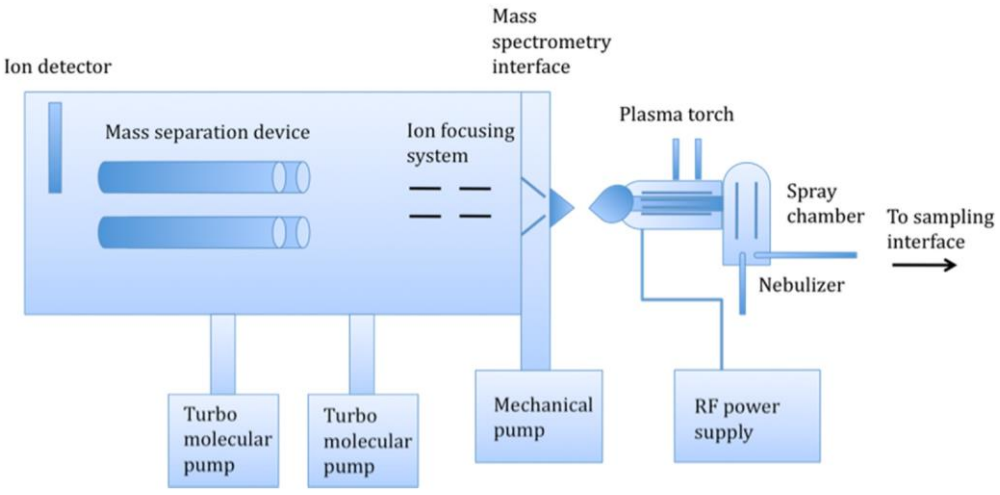

Figure 3. 4: The basic components of an ICP-MS system (Madzunya *et al.*, 2021).

3.4 Sample preparation

Sample digestion using microwave digestion system

The samples were dissolved using a Perkin-Elmer computerized Titan microwave digestive system (Acid digestion) shown on figure 3.5. The samples (Figure 3.6 A) were weighed at a

mass of 0.5 g and poured into a microwave digester vessel (75 ml standard pressure). The vessels were filled with 2.0 mL of purified water, 2.0 mL of concentrated HNO_3, 6.0 mL of concentrated HCl, and 0.5 mL H_2O_2. The vessels containing the samples were placed within the Perkin-Elmer microwave digestion system, sealed into the rotor, and heated for a maximum of 30 minutes at 180 ^oC and 50 KPa pressure (do AMARAL *et al.*, 2016). For chemical separation, an aqueous solution (Figure 3.6 B) in the acidified matrix was obtained.

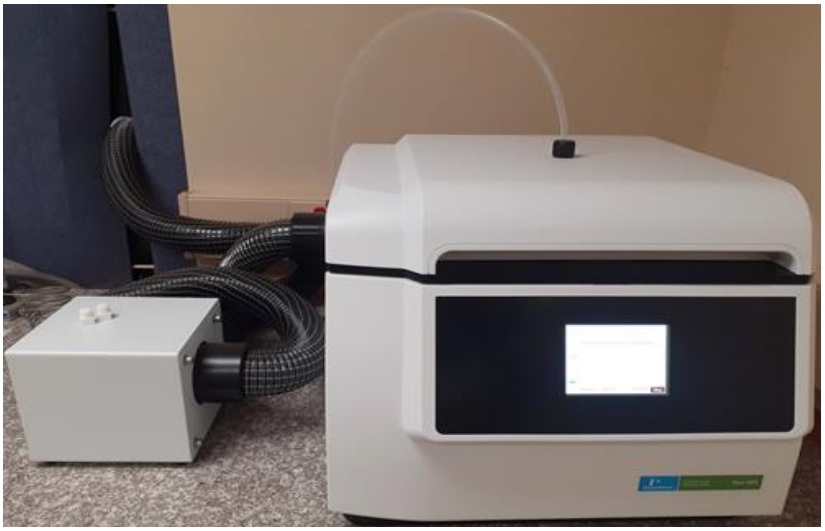

Figure 3. 5: Perkin-Elmer Titan Microwave digester.

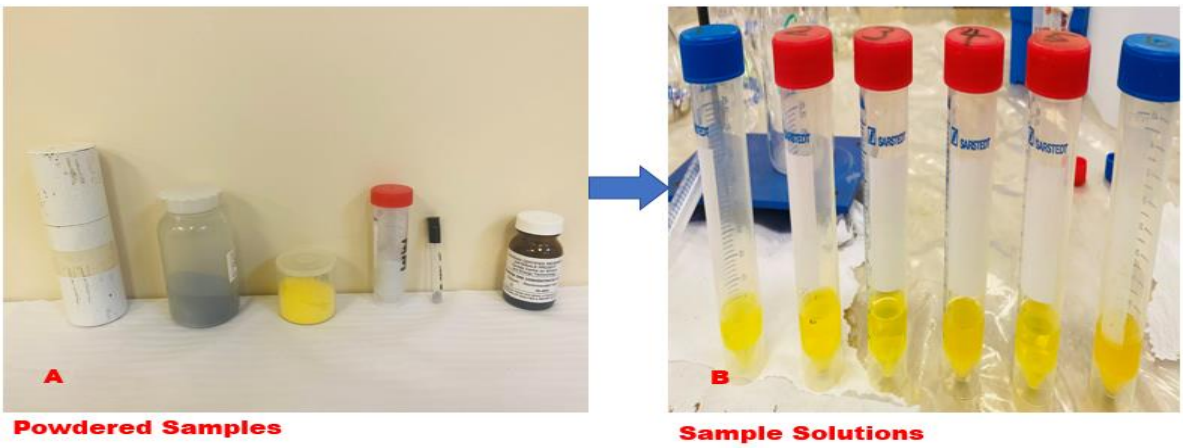

Figure 3. 6: Digestion procedure for sample preparation.

Sample separation method and sample analysis on ICP-MS

The main goal of the chemical separation technique was to remove the bulk of uranium from the sample to avoid contamination of the measurement equipment. TRU^{TM} resin was chosen

for REE/uranium separation because it has good uranium adsorption properties as shown on sample separation procedure on Figure 3.7. TRU^{TM} resin (1.6 L) was preconditioned with ultrapure water and 10 mL of 2 M HNO_3 in a polytetrafluoroethylene (PTFE) column closed with cotton wool (10 mL). 300 µL of prepared samples (Figure 3.6 B) was diluted four-fold using ultra-pure water (100 µL) in order to adjust proper HNO_3 concentration. The sample aliquots were loaded into the resin column. The sample tube was washed two times with 1 mL of 2 M HNO_3 added to the sample load (Krajko, 2016). The load sample solution was removed then added a new Teflon beaker for tripling rare earth elements. 1 mL of concentrated hydrochloric acid (HCL) and 4 mL of 4 M HCL was added to the sample. To remove any remaining organic resin, the samples were evaporated almost completely dry on a hotplate. After evaporation was complete, 200 µL of ultra-pure HNO_3 was added to the final fractions. The samples were heated slightly and the residue was dissolved in 1 mL of 2% (m/m) ultra-pure nitric acid before being analysed by ICP-MS (Krajko, 2016).

The auto-sampler was loaded with the prepared blank samples, calibration standard, and quality control samples for ICP-MS measurement and calibration. For the analysis of rare earth elements, a custom-made multi-element standard were used. The ULTRA SPEC multi-element aqueous CRM (CRM004) standard solution contained 1000 µg/ml of Ce, Dy, Er, Eu, Gd, Ho, La, Nd, Pr, Sc, Sm, Tb, Y, Yb. The instrument was operated by using the Syngistix software.

For each set of measurements, the TotalQuant analysis method was utilized, and it was programmed to execute a blank and a standard check every 10 samples. Each sample was analysed in replicates of 10 with the instrument working parameters shown in Table 3.1.

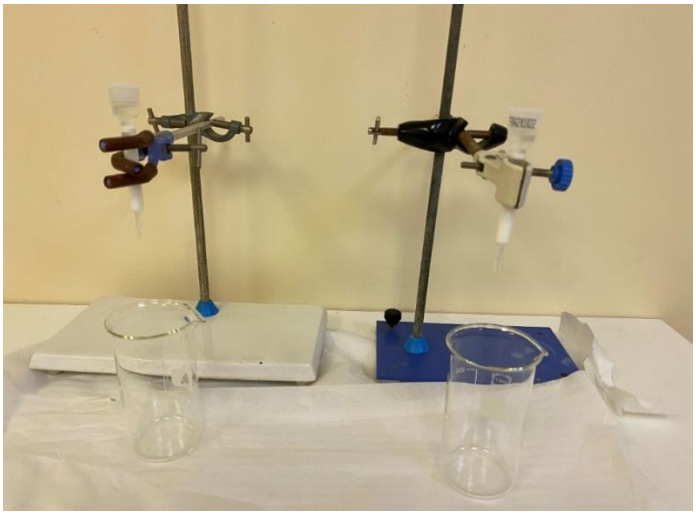

Figure 3. 7: Sample separation procedure.

TABLE 3. 1: Instrument working parameters.

Description	**Values**
Nebulizer Gas Flow [NEB]	0,94
AMS Gas Flow	0
Auxiliary Gas Flow	1,2
Plasma Gas Flow	15
ICP RF Power	1600
Analog Stage Voltage	-2912
Pulse Stage Voltage	1700
Discriminator Threshold	12
Deflector Voltage	-11,5
Quadrupole Rod Offset [QRO]	-2
Cell Entrance Voltage	-4
Cell Exit Voltage	-4
Cell Rod Offset [CRO]	-10

3.5. Statistical analysis

There are numerous statistical tools available for the analysis of multivariate data. These include discriminant function analysis (DFA), principal component analysis (PCA), and cluster analysis (CA) (Ntsohi, 2019). However, the data for this specific study were subjected to an analysis of variance (ANOVA) with a significant value (p=0,05) (Connelly, 2021). ANOVA does not reveal which groups differ significantly; it only assesses whether there is a statistical difference between groups. In other words, if the test is significant, it implies that at least one pair of means is different, but it is ambiguous as to which pair or pairs (Connelly, 2021). The dependent variable in a one-way ANOVA is continuous, such as the prevalence of medication errors, and the independent variable is categorical, such as before and after the implementation of various interventions, such as steps to lower medication errors (Assaad *et al.*, 2014; Connelly, 2021). Several concepts form the foundation of a one-way ANOVA. First, it is thought that each sample was selected independently without consideration of other samples

(sample independence). In other words, when the samples are unconnected in any manner, such as when they originate from the same people on different dates, alternate testing are available. In addition, data variation on the dependent variable must become comparable across groups (variance equality) (Connelly, 2021). The last presumption is that each sample comes from a population that is regularly distributed (normality) (Connelly, 2021). There exist tests for normalcy and variance equality, however, these outcomes are frequently not published in studies. Inaccuracies in these presumptions could render the statistic's findings invalid.

An F ratio (or simply F) is the result of this statistical test, which is the ratio of the degree of variation between the groups to the degree of variation within the groups (Polit & Beck, 2020). The ratio of the Mean of Squares within Groups (MSW) to the Mean of Squares between Groups (MSB) is the F-test value (Mishra *et al.*, 2019). Equation 13 shows F-test ratio:

$$F = \frac{MS_B}{MS_W} \qquad (13)$$

If the null hypothesis were true, there would be no difference between the groups, therefore the ratio would be near to one. The larger the value of F, the more likely it is that the difference between the groups on the independent variable is real (Connelly, 2021; Mishra *et al.*, 2019). The means of the groups were sufficiently different from one another for the difference to be significant if the *p*-value is (<0.05). The degrees of freedom are also included in the test findings (number of participants minus 1). After the *F*, this is typically written in paraphrase (Emerson, 2019). Researchers must perform additional post hoc tests or multiple comparison techniques to determine which data sets are statistically distinct (Polit & Beck, 2020). In essence, the number of additional tests needed to prevent Type I mistakes reduces the alpha level (*p*-value) (Grove *et al.*, 2012). The Scheff, Dunnett, and Tukey HSD tests are often employed tests; each is utilized in a distinct situation (Mishra *et al.*, 2019). For this study, four independent groups (mines) and 14 REE variables made up the data set. Due to confidentiality agreements, the mines were referred to as W1, W2, W3, W4, W5, and W6 for UOC1, UOC2, UOC3, UOC4, Uore1, and Uore2, respectively.

CHAPTER 4: RESULTS AND DISCUSSION

4.1 Introduction

In the twenty years from the start of research and development, nuclear forensic science has undergone significant improvements in both the analytical techniques used and the interpretation of the resulting data. Characterizing the chemical and isotopic characteristics of UOCs and uranium ore in order to identify the material's original source and determine where it was diverted from. Regulatory control is a major research focus of nuclear forensic investigations. The aim of this project was to determine REE in uranium bearing material for nuclear forensics purposes using ICP-MS.

The research's findings are categorized into three groups:

- REE concentrations analysis using ICP-MS
- REE CI-chondrite normalized patterns analysis
- Statistical evaluation of REE data

4.2 REE Concentration of uranium samples

4.2.1 Analysis of UOC samples

The REE concentration of the analysed uranium ore concentrate samples are presented in Table 4.1. Promethium (Pm) is reported as REE but is the rarest and only appears in minute amounts in natural materials because it lacks long-lived or stable isotopes. The light REE (La, Ce, Pr, Nd, Sm) and heavy REE (Eu, Gd, Tb, Dy, Ho, Er, Tm, Yb, Lu, Sc) were analysed (John *et al.*, 2021; Patah *et al.*, 2021). The ΣREE concentrations in Table 4.1 ranged from 180,106 ppb to 15585,068 ppb. As a result, Hany and Mervat stated previously that the ΣREE concentration in the alkaline rocks of Abu Khuruq varied from 35,18 ppb to 1075,58 ppb, which is lower than the investigated samples (El-Gamal & El-Haddad, 2019). The concentration range of the REE for lutetium (Lu) showed the lowest concentration (2,213 ± 0,178 ppb) while Cerium (Ce) showed the highest concentration (4564, 787 ppb ± 14,227 ppb) for all UOC samples, respectively. For UOC1, the REE concentration ranges from 2,213 ± 0,178 ppb (Lu) to 212,148 ± 1,704 ppb (Ce), with a mean of 27,435 ppb and a standard deviation of 19,255. For UOC2, the concentration ranged from 1,412 ± 0,030 ppb (Lu) to 636,808 ± 2,608 ppm (Ce) with a mean of 70,015 ppb and a standard deviation of 16,359. UOC3 concentration ranged from 1,882 ± 0,091 ppb (Lu) to 131,382 ± 1,018 ppb (Ce), with a mean of 12,865 ppb and a standard deviation of 9,052 ppb, while UOC4 concentration ranged from 54,663 ± 0,397 ppb (Lu) to

1808,643 ± 4,783 ppb (Ce), with a mean of 1113,219 ppb and a standard deviation of 156,448 ppb**.** The ΣLREE concentration range from 168,378 ppb to 12044,952 ppb, while heavy REE concentrations (ΣHREE) range from 17,366 ppb to 3589,589 ppb for all the UOC samples.

These outcomes are to be expected given that light REE are more prevalent than heavy REE, which are typically less abundant but more valued and economically viable than light REE (Patah *et al.*, 2021). In line with the Oddo-Harkins principle, REE concentrations tend to decrease as atomic number increases Ce > La > Pr > Sm > Gd > Dy > Er > Yb > Eu > Tb > Ho > Tm > Lu (El-Gamal & El-Haddad, 2019; John *et al.*, 2021). The order of the average REE concentrations in the samples analysed was La> Ce> Nd > Sm > Pr > Gd > Dy > Er > Yb > Eu > Ho > Tb > Tm > Lu. There were a few exceptions, though (i.e., Dy enrichment and Eu depletion). The sample's ΣLREE/HREE ratio showed a range of values, which is supportive of LREE enrichment.

Figure 4.1 to 4.4 in page 51 and 52 shows a bar graphs of heavy and light REE concentrations in all samples (UOC1, UOC2, UOC3 and UOC4) in ppb. Similar patterns with variable concentrations were visible in the REE bar graphs for UOC1 and UOC2. Although at various concentrations, the higher peaks for cerium (Ce), lanthanum (La), and neodymium (Nd) are skewed to the left and show the presence of light-REE characteristics. The statistical significance of these variations might be ascertained using ANOVA or the F-test on the dataset. The statistical analysis of these findings is discussed in more details in Section 4.4.

Table 4. 1: Rare earth elements (REE) concentration (ppb) from uranium ore concentrate samples.

REE	UOC1	UOC2	UOC3	UOC4
La	25,161 ± 0,301	96,684 ± 0,386	6,352 ± 0,108	1808,643 ± 4,783
Ce	212,148 ± 1,704	636,808 ± 2,608	131,382 ± 1,018	4564,787 ± 14,227
Pr	9,770 ± 0,233	28,063 ± 0,136	3,458 ± 0,121	477,385 ± 2,292
Nd	48,521 ± 0,756	135,836 ± 1,012	12,230 ± 0,240	2435,693 ± 8,771
Sm	14,572 ± 0,470	23,400 ± 0,308	3,520 ± 0,170	1014,560 ± 2,863
Eu	4,232 ± 0,194	5,141 ± 0,083	2,777 ± 0,098	80,621 ± 0,310
Gd	20,794 ± 0,434	22,097 ± 0,177	3,969 ± 0,160	1624,891 ± 5,126
Tb	4,542 ± 0,238	3,540 ± 0,057	2,611 ± 0,165	276,142 ± 0,986
Dy	18,698 ± 0,520	12,856 ± 0,132	3,177 ± 0,186	1762,518 ± 3,388
Ho	4,361 ± 0,234	2,898 ± 0,048	2,250 ± 0,128	260,518 ± 1,275
Er	8,290 ± 0,292	5,138 ± 0,059	2,139 ± 0, 109	633,840 ± 2,355
Tm	2,533 ± 0,184	1,677 ± 0,037	1,987 ± 0,107	83,206 ± 0,447
Yb	8,258 ± 0,349	4,661 ± 0,100	2,372 ± 0,163	507,601 ± 2,253
Lu	2,213 ± 0,178	1,412 ± 0,030	1,882 ± 0,091	54,663 ± 0,397
Mean value	27,435	70,015	12,865	1113,219
STD	19,255	16,35975	9,052	156,448
STD ERR	6,089	5,173	2,862	49,473
ΣLREE	339,290	952,739	168,378	12044,952
ΣHREE	50,892	32,645	17,366	3589,589
ΣREE	384,093	980,211	180,106	15585,068
ΣLREE/ΣHREE	6,667	29,184	9,696	3,356
La_N/Yb_N	2,113	14,362	1,854	2,467
Gd_N/Yb_N	2,088	3,919	1,383	2,646
La_N/Gd_N	1,012	3,665	1,341	0,932
Ce/Ce^*	3,257	2,931	6,721	1,178
Eu/Eu^*	0.727	0,676	2,220	0,1888

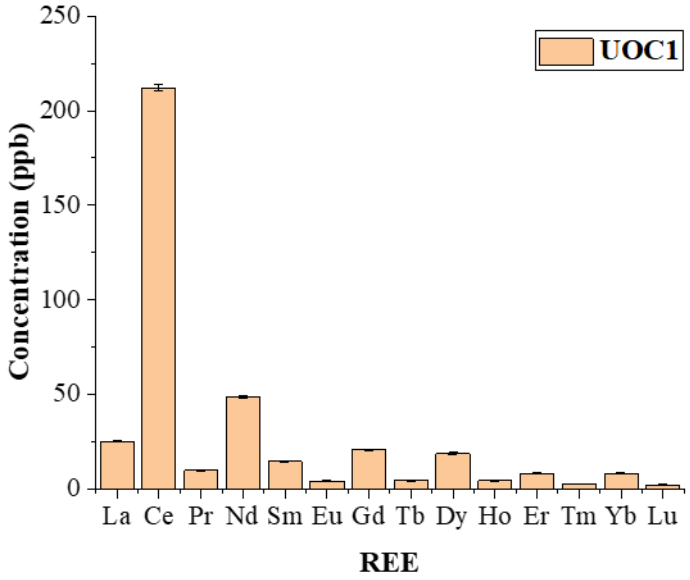

Figure 4. 1: Bar graph of REE concentration for UOC1

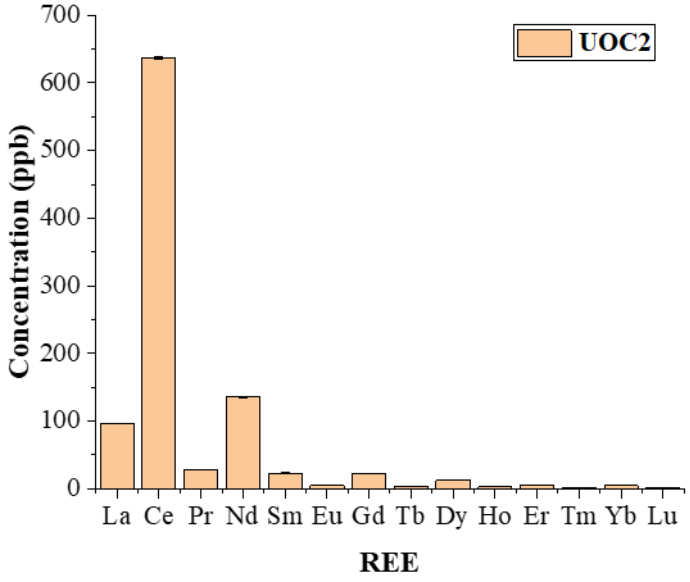

Figure 4. 2: Bar graph of REE concentration for UOC2

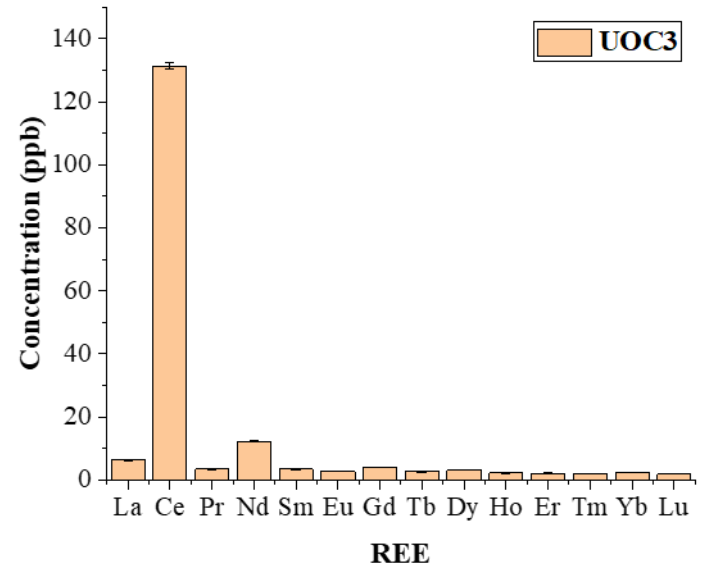

Figure 4. 3: Bar graph of REE concentration for UOC3

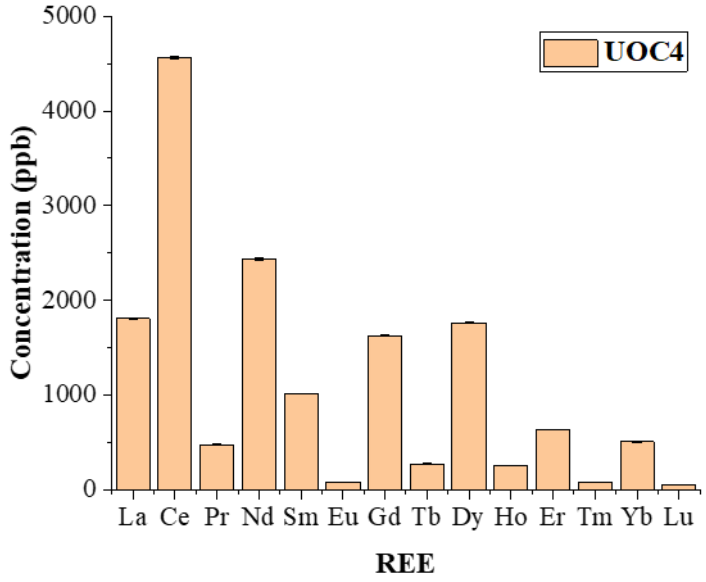

Figure 4. 4: Bar graph of REE concentration for UOC4

4.2.2 Analysis of uranium ore samples

The REE concentration of the analysed uranium ore samples are given in Table 4.2 in page 54. The ΣREE concentrations of the analysed samples ranged from 8388,788 ppb to 12442,041 ppb for U ore 2 and U ore1 respectively. This ores shows higher REE concentration than Gua

Musang samples which had concentration ranging from 79,7913 ppb to 574,3858 ppb (Shafiee *et al.*, 2020). Lutetium (Lu) shows the lowest concentration, while cerium (Ce) showed the highest in each of the for sample. The concentration of REE ranged from 3,043 ± 0,037 ppb (Lu) to 6001,318 ± 18,808 ppb cerium (Ce) for U ore1 with a mean of 888,710 ppb and a standard deviation of 140,339, while the concentration of U ore2 ranged from 10,813 ± 0,063 ppb (Lu) to 3664,804 ± 10,318 ppb (Ce) with a mean of 599,199 ppb and a standard deviation of 78,590. These concentration values were greater than those reported by (John *et al.*, 2021), for the Nigerian uranium ore, which ranged between 0.020 ppb (Lu) and 2.888 ppb (Ce) which showed similar characteristics with the observed.

The ΣLREE concentration ranged from 7809,616 ppb to 12328,192 ppb, whereas the total concentrations of heavy REEs (ΣHREE) ranged from 158,227 ppb to 604,024 ppb for both ore respectively. Cerium (Ce), neodymium (Nd), and lanthanium (La) appear to be the most prevalent elements in all samples. This is shown in Figures 4.5 and 4.6 respectively on page 55. As mentioned in the above section, the light REE are more prevalent than heavy REE, which are typically less abundant but more valuable and commercially feasible than light REE, these results are to be expected. The Oddo-Harkins rule states that as the atomic number rises, REE concentrations tend to decrease (Zepf, 2013). Statistical significance of these variations was also tested using one-way ANOVA. The statistical results are presented in section 4.4.

Table 4. 2: Rare earth elements (REE) concentration (ppb) from uranium ore samples

REE	U ore1	U ore2
La	2554,933 ± 8,521	1537,777 ± 4,429
Ce	6001,318 ± 18,808	3664,804 ± 10,318
Pr	550,594 ± 1,838	331,816 ± 1,059
Nd	2451,444 ± 9,517	1503,271 ± 4,195
Sm	390,314 ± 2,937	317,537 ± 1,139
Eu	55,592 ± 0,240	60,889 ± 0,465
Gd	280,977 ± 1,159	370,932 ± 0,985
Tb	23,042 ± 0,179	52,827 ± 0,218
Dy	77,152 ± 0,569	293,909 ± 0,876
Ho	9,978 ± 0,085	41,536 ± 0,211
Er	21,022 ± 0,231	98,873 ± 0,378
Tm	3,786 ± 0,038	14,676 ± 0,122
Yb	18,846 ± 0,220	89,128 ± 0,394
Lu	3,043 ± 0,037	10,813 ± 0,063
Mean value	888,710	599,199
STD	140,339	78,590
STD ERR	44,379	24,852
ΣLREE	12328,192	7809,616
ΣHREE	158,227	604,024
ΣREE	12442,041	8388.788
ΣLREE/ΣHREE	77,914	12,929
La_N/Yb_N	93,864	11,946
Gd_N/Yb_N	12,323	2,430
La_N/Gd_N	7,617	5,435
Ce/Ce^*	1,213	1,230
Eu/Eu^*	0,502	0,530

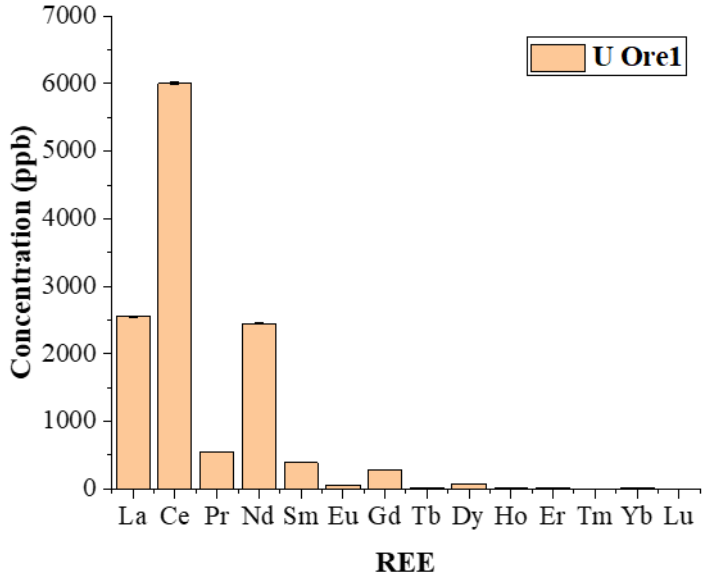

Figure 4. 5: Bar graph of REE concentration for UOre1

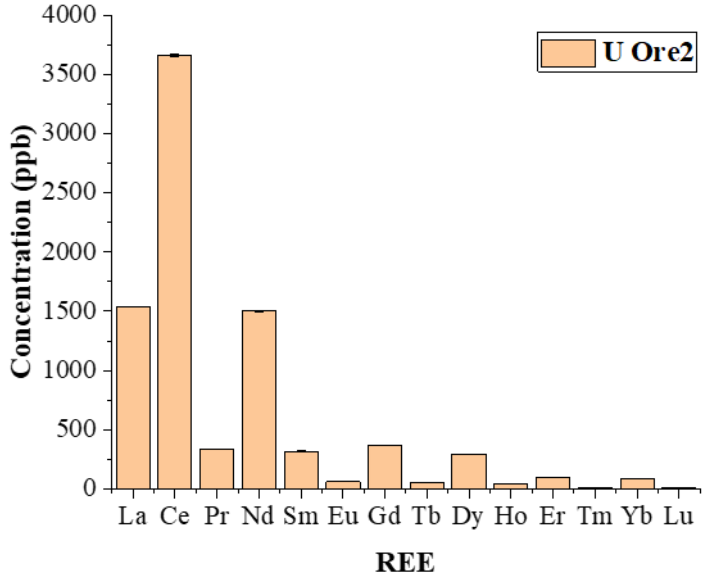

Figure 4. 6: Bar graph of REE concentration for UOre2

4.3 Signatures of REE relative to C1-chondrite

4.3.1 Uranium ore concentrate (UOC)

Figures 4.7 to 4.10 show REE trends of the analysed UOC samples. Identifying signatures that could contribute to a nuclear forensic library was the focus of this research. The literature states that the origin affects the REE concentrations (Spano *et al.*, 2017). The REE concentrations

are standardized to the chondrite values of Anders and Grevesse for better comparability in order to meet the objectives (Cates *et al.*, 2013). According to (Bau *et al.*, 2014) and (Dai *et al.*, 2015), rare earth elements have been used for a long time as geochemical indicators of the sedimentary environment and post-sedimentary history of coal deposits because of their coherence behaviour during various geochemical processes and their predictable pattern of fractionation. Comparisons of REE patterns are facilitated by the normalization and parameters described below. After chondrite standardization, La_N, Gd_N, and Yb_N are obtained.

Their ratios can indicate one of the three rare earth element enrichment types in all samples. The fractionations of LREE to HREE, LREE to MREE, and MREE to HREE are used to represent La_N/Yb_N , La_N/Gd_N , and Gd_N/Yb_N ratios respectively (Brito *et al.*, 2021). The formulas for the Ce and Eu anomalies are, $Ce/Ce^* = Ce_N/(La_N/Pr_N)^{0.5}$ and $Eu/Eu^* = Eu_N/(Sm_N/Gd_N)^{0.5}$. REE concentrations are normalized data, which is indicated by the subscript N (normalised values) in the parameters above (Liu *et al.*, 2019). La_N/Gd_N (1,012) and Gd_N/Yb_N (2,088) showed that the enrichment of MREE to HREE was more pronounced than the enrichment of LREE to MREE in UOC1 (Figure 4.7, page 57). The same Figure further displayed the enrichment of LREE that contained a very slight negative Eu anomaly (Eu/Eu* = 0,721) with a positive Ce anomaly (Ce/Ce* = 3,257). Significant fractionation between MREE and HREE is normally indicated by a high Gd_N/Yb_N ratio.

UOC2 (Figure 4.8, page 58) demonstrated a notable enrichment of LREE (La_N/Yb_N = 14,362) and depletion of HREE (Gd_N/Yb_N = 3,919), as well as a negative Eu-anomaly (Eu/Eu* = 0.676) and a positive Ce anomaly (Ce/ Ce* = 2,931). The characteristics of UOC3 (Figure 4.9 page 59) included HREE depletion (La_N/Yb_N = 1,854, Gd_N/Yb_N = 1,383), pronounced positive Ce anomalies (Ce/ Ce* = 1,672), and moderate positive Eu anomalies (Eu/Eu* = 2,220). UOC4 (figure 4.10, page 59) showed a distinct HREE enrichment (Gd_N/Yb_N = 2,646), a depleted LREE (La_N/YbN = 2,467), a significant positive Ce anomaly (Ce/ Ce* = 1,672), and a slight negative Eu anomaly (Eu/Eu* = 0,1888). The studied UOC4 REE distribution pattern was very similar to that of Riruwai mine in Nigeria (John *et al.*, 2021). Both consisted of enriched HREE, depleted LREE and a strong negative Eu anomaly. UOC1, UOC2, and UOC3 were all enriched for LREE (LaN/YbN), according to Table 4.1, with UOC2 having the greatest value.

The normalized pattern in Figure 4.8, page 58 resembled those of PAAS and UCC, with LREEs being enriched relative to HREEs (LaN/YbN ranged from 6.5 to 29.3), HREEs having relatively flat patterns (GdN/YbN ranged from 1.0 to 3.8), and the concentration of REEs

continuously decreasing with increasing atomic number (Kritsananuwat *et al.*, 2015). UOC4 shows depleted LREE and enriched HREE. UOC4 included the lowest GdN/YbN (MREE/HREE) value, 0,188 for Eu/Eu*, and a value of Ce/Ce* (1.178). (Varga *et al.*, 2010) revealed that quartz-pebble conglomerate (QPC) or placer deposits have a negative Eu anomaly and are therefore from a plagioclase-rich source, allowing for Eu substitution with calcium (Ca).

In comparison to UOC1, UOC2 and UOC4, UOC3 had the greatest Eu/Eu* ratio (2,220) and Ce/Ce* ratio (MREE/HREE) values. The vein deposits (UOC) of Eldorado and Gunnar displayed a negative Eu anomaly, in UOC1, UOC2 and UOC4 examined in this study, which may be connected to the reducing circumstances during the precipitation of uranium oxides (Mercadier *et al.*, 2011). Additionally, as the vein progressed, it may have come into contact with plagioclase-rich country rock, which led to gradual Eu replacement with Ca along the vein. UOC3 also had a moderate La_N/Yb_N (MREE/HREE) ratio. The highest Gd_N/Yb_N (MREE/HREE) ratio could be found in UOC2, which also had a moderate Eu/Eu* value of 0.676. La_N/Gd_N and Gd_N/Yb_N ratios were used to determine the degrees of LREE and HREE respectively (Wang & Liang, 2015). The degree of HREE fractionation, with Gd_N/Yb_N values of UOC1 (2,088), UOC2 (3,919), UOC3 (1,383) and UOC4 (2,646), was slightly greater than that of LREE fractionation, with the $(La/Gd)_N$ values of UOC1 (1,012), UOC2 (3,665), UOC3 (1,341) and UOC4 (0,932).

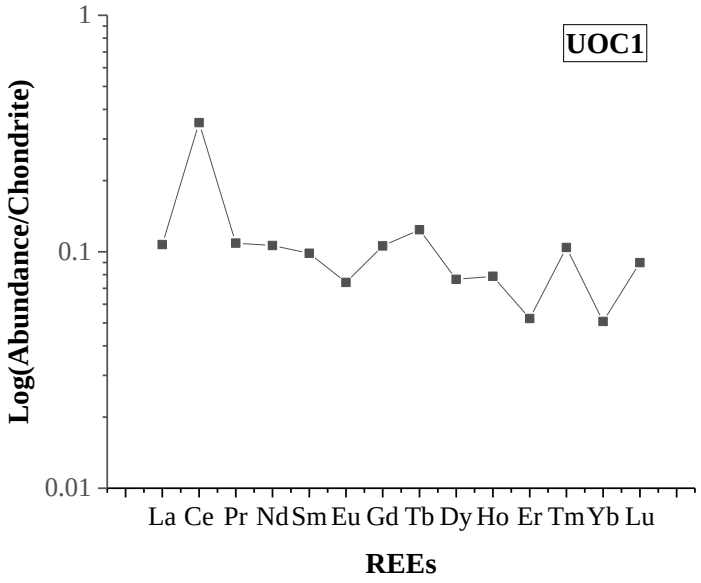

Figure 4. 7: C1 chondrite normalized REE patterns for UOC1

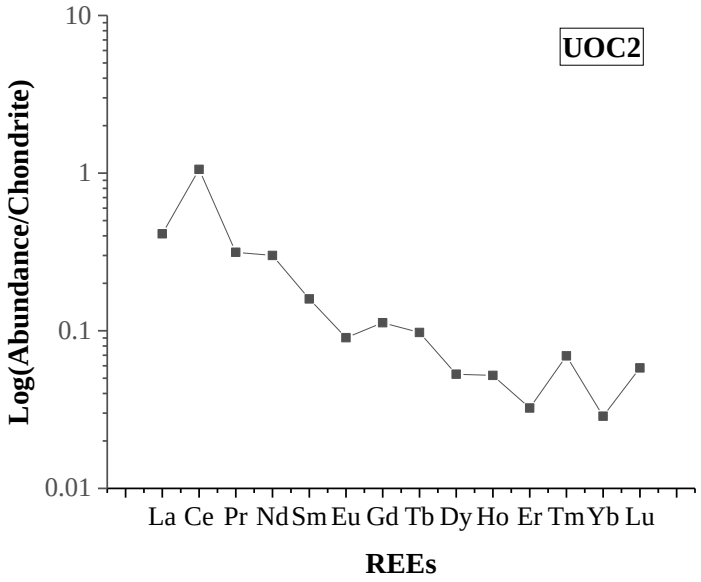

Figure 4. 8: C1 chondrite normalized REE patterns for UOC2

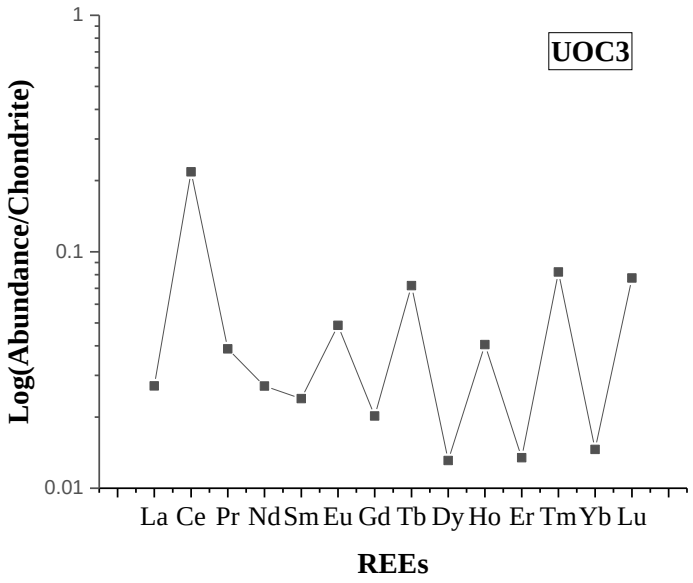

Figure 4. 9: C1 chondrite normalized REE patterns for UOC3

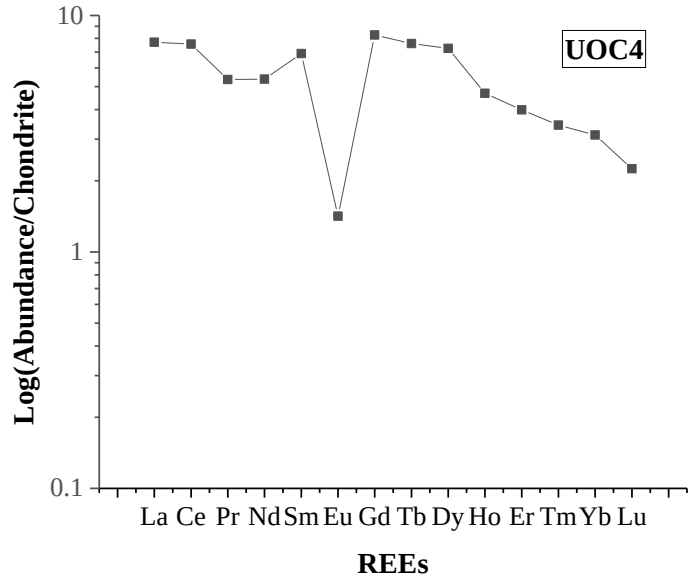

Figure 4. 10: C1 chondrite normalized REE patterns for UOC4

4.3.2 Uranium ore samples

Figures 4.11 and 4.12, pages 60 and 61 respectively showed the constancy of the geochemical distribution of REEs, and was demonstrated by the two normalized REE patterns of uranium

ore samples (Wang & Liang, 2015). However, LREE enrichment and HREE depletion were observed in the REE patterns, the curves extending downward from left to right, a negative Eu anomaly, and a positive Ce anomaly. Due to their significantly larger ionic radii than HREEs, LREEs may have higher levels of enrichment (Balboni *et al.*, 2017). Uore1 showed a considerable enrichment of LREE and depletion of HREE, as well as a negative Eu-anomaly (Eu/Eu* = 0.502) and a positive Ce anomaly (Ce/ Ce* = 1,213). Studies carried out at the Namibia uranium mines (Madzunya *et al.*, 2021) revealed that LREE (La_N/Yb_N) concentration of uranium ore was lower than the investigated concentration of Uore1, which were as follows: 8.55 (M1), 4.62 (M2), and 2.67 (M3). The observed characteristic are comparable to that of younger granites, which exhibited LREE-enrichment with Lan/Ybn values between 5.28 and 13.46, highly fractionated LREE, flat heavy REE patterns, and moderately to strongly negative Eu anomalies (El Bahariya, 2019). While ore from various deposits, including the breccia deposit at the Olympic Dam Mine in Australia, showed a positive Eu anomaly in the REE pattern, intrusive non-granitic associated deposits were characterized by both positive Ce and negative Eu anomalies (Corcoran *et al.*, 2019).

Uore2 $(La/Gd)_N$ ratio had a value of 5,435 (Table 4.2), which indicated that LREE had a high degree of internal fractionation, while $(Gd/Yb)_N$ ratio had a value of 2,430, which indicate that HREE had a low degree of internal fractionation. Similarly, the degree of LREE fractionation of La_N/Gd_N were slightly higher for 3.36 (M1), 3.33 (M2), and 2.62 (M3) than for HREE fractionation (Madzunya *et al.*, 2021). Uore2 exhibited LREE enrichment (La_N/Yb_N = 11,946), a very faintly negative Eu anomaly (Eu/Eu* = 0,530), and a positive Ce anomaly (Ce/Ce* = 1,230). Rocks from Namibia's Damara Orogen also showed similar relative flat plots with large negative Eu anomalies in their CN patterns (Falster *et al.*, 2018). In mostly sandstone-hosted roll front/calcrete uranium deposits reported in Botswana, a negative Eu anomaly was compatible with the mineralization fluids linked to granitic hydrothermal melting or weathered granitic deposits (Ntsohi *et al.*, 2021; Varga *et al.*, 2010). The variations in the mineralizing processes and geological settings between different types of uranium deposits was closely related to the specific REE signature in uranium oxides (Mercadier *et al.*, 2011).

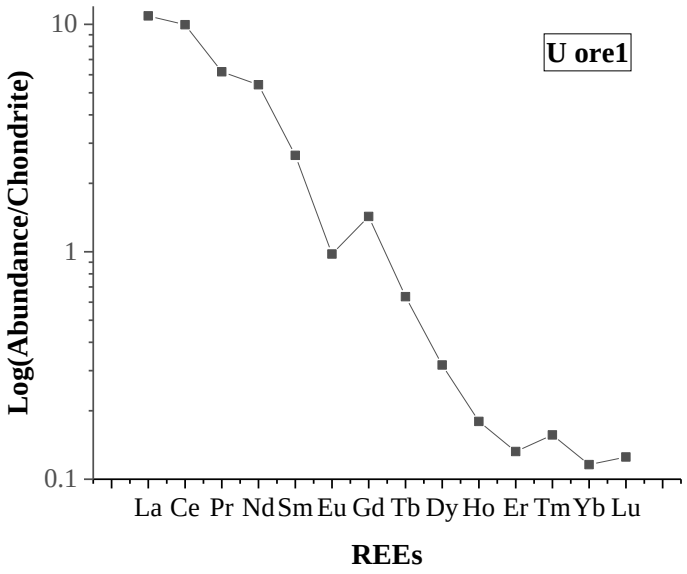

Figure 4. 11: C1 chondrite normalized REE patterns for UOre1

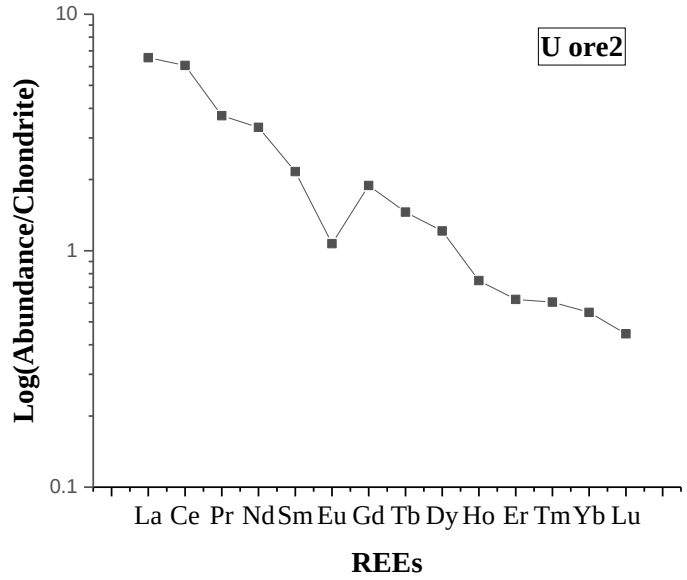

Figure 4. 12: C1 chondrite normalized REE patterns for UOre2

4.4 Statistical Evaluation of REE data

One-way ANOVA can be carried out using several software programs, including R, SAS, JMP, and SPSS (Assaad *et al.*, 2014). Statistical Package for the Social Sciences (SPSS) version 25 was used to conduct the statistical analysis (IBM). To determine whether the differences observed in the outcomes of the test samples under inquiry were statistically

significant, ANOVA was performed on the REE data. In this study, it was utilized to identify which of the elements of the samples' impurity spectrum changed considerably depending on the sampling site (origin). The overall variance of the data set was divided into two components for ANOVA: the variance within each sample group and the variance between the various sample groups.

Tables 4.3 and 4.4 show the samples' F-values, significant P-values, and F-critical values. The results were obtained from the study of the REE of the UOC and uranuim ore samples. The nuclide discovered had F-values that were higher than the F-critical value. All elements have p-values less than 0.05, which indicates very strong evidence of sample differences and indicating that variations in measured values were not the result of chance. As a result, the REE elements in this investigation were statistically significant. They can be utilized as a strong signature in nuclear forensic investigations and added to the South African Nuclear Library.

Table 4. 3: Statistical Analysis of the UOC samples using REE.

REE	F-Value	F-Critical	P-Value
La	135095.27	2.86	0.001
Ce	85185.44	2.86	0.001
Pr	40334.44	2.86	0.001
Nd	71626.62	2.86	0.001
Sm	117297.75	2.86	0.001
Eu	39029.04	2.86	0.001
Gd	97642.16	2.86	0.001
Tb	70119.60	2.86	0.001
Dy	259794.44	2.86	0.001
Ho	38980.67	2.86	0.001
Er	70001.78	2.86	0.001
Tm	26648.66	2.86	0.001
Yb	48251.24	2.86	0.001
Lu	14077.69	2.86	0.001

Table 4. 4: Statistical Analysis of the Uranium Ore samples using REE.

REE	F-Value	F-Critical	P-Value
La	73.39	4.41	0.001
Ce	73.32	4.41	0.001
Pr	72.78	4.41	0.001
Nd	72.42	4.41	0.001
Sm	41.99	4.41	0.001
Eu	59.72	4.41	0.001
Gd	90.38	4.41	0.001
Tb	84.51	4.41	0.001
Dy	83.20	4.41	0.001
Ho	82.50	4.41	0.001
Er	81.58	4.41	0.001
Tm	80.16	4.41	0.001
Yb	81.36	4.41	0.001
Lu	78.26	4.41	0.001

CHAPTER 5: CONCLUSIONS

This project's primary goal was to identify and quantify REE in uranium-bearing materials in order to conduct precise and accurate analysis. Rare earth element concentration in UOC and uranium ore has been determined. The process, which involves the efficient chemical separation of lanthanides using TRU^{TM} extraction chromatography resin and ICP-MS analysis, provides numerous advantages over simple analyte measurement, particularly when analysing REE in complex matrixes at the trace level. Using the aforementioned procedures, the interference-free solution was used to precisely determine the presence of trace REEs. It provided a straightforward method for quickly determining REEs in uranium-rich samples and is advised for all varieties of uranium-rich materials. The isotopic spectrum patterns of the REEs, which were chondrite normalized and reported, varied amongst sample locations. The REEs concentration dataset was put through an ANOVA test, and the results provided enough differentiation between the mines. Four (4) UOC samples and two (2) uranium ores were determined, and it was observed that all rare-earth elements were present in all analysed samples.

The study suggests that the pronounced negative Eu anomalies, enriched LREE, depleted HREE, and higher fractionation of LREE compared to HREE observed are a nuclear forensic signature for the South African uranium ore deposits. The uranium ore samples showed comparable REE patterns with flat HREE and pronounced negative Eu anomalies. While $(Gd/Yb)_N$ ratio has a value of 2,430, which suggests that HREE has a low degree of internal fractionation. Uore2 revealed that LREE has a significant degree of internal fractionation.

The analysis of uranium ore samples analysed in ANOVA revealed that the REEs are distinctive enough to differentiate between the mining sites, moreover they are statistically significant. The chondrite normalization patterns varied among all UOC samples. REE concentrations in UOC1, UOC2, UOC3, and UOC4 ranged from 180,106 ppb to 15586,068 ppb, with UOC4 having the highest value and UOC3 having the lowest. While UOC1 through UOC3 demonstrated enriched LREE (La_N/Yb_N), UOC4 displayed depleted LREE. UOC1, UOC2, and UOC4 showed negative Eu anomalies based on the ratios, although sample UOC3 showed a positive anomaly. Additionally, all samples showed negative Ce anomalies. It was revealed that quartz-pebble conglomerate (QPC) or placer deposits have a negative Eu anomaly and are consequently from a source that is rich in plagioclase, allowing for the replacement of Eu with Ca. This occurs because granitic melt or weathered granitic

deposits, such those in the Blind River/Elliot Lake region of Canada, interact with the REE mineralizing fluids. In comparison to LREE fractionation, HREE fractionation was slightly more pronounced.

According to the analysis of UOC done in ANOVA, the REEs are statistically significant and distinguishable enough to be used to distinguish between mining sites. According to the study, ICP-MS has the potential to be a technique for identifying and measuring rare earth elements in geological samples. Nuclear forensic techniques are crucial instruments for confirming the claimed provenance of uranium-bearing materials. Additionally, they can be used to characterize or trace the source of UOC/Uranium ore seized from illegal trafficking.

REFERENCES

Agency, I.A.E.A 2009. *Nuclear Fuel Cycle Information System*. Paper presented at the IAEA-TECDOC-1613, VIENNA.

Agency, I.A.E.A 2015. *Advances in Nuclear Forensics: Countering the Evolving Threat of Nuclear and Other Radioactive Material Out of Regulatory Control: Summary of an International Conference Organized by the International Atomic Energy Agency and Held in Vienna, 7-10 July 2014*. International Atomic Energy Agency.

Aggarwal, S.K. 2016a. Nuclear forensics: what, why and how? *Current Science*:782-791.

Aggarwal, S.K. 2016b. Thermal ionisation mass spectrometry (TIMS) in nuclear science and technology–a review. *Analytical Methods*, 8(5):942-957.

Aggarwal, S.K. 2016c. Alpha-particle spectrometry for the determination of alpha emitting isotopes in nuclear, environmental and biological samples: past, present and future. *Analytical methods*, 8(27):5353-5371.

Al-Hakkani, M.F. 2019. Guideline of inductively coupled plasma mass spectrometry "ICP–MS": fundamentals, practices, determination of the limits, quality control, and method validation parameters. *SN Applied Sciences*, 1(7):1-15.

Apostol, A. & Maliuk, I. 2016. Uranium Isotopic Composition Analysis using Gamma Spectrometry: Applications in Nuclear Forensics. *Romanian Reports in Physics*, 68(2):822-831.

Asai, S. & Limbeck, A. 2015. LA-ICP-MS of rare earth elements concentrated in cation-exchange resin particles for origin attribution of uranium ore concentrate. *Talanta*, 135:41-49.

Assaad, H.I., Zhou, L., Carroll, R.J. & Wu, G. 2014. Rapid publication-ready MS-Word tables for one-way ANOVA. *SpringerPlus*, 3(1):1-8.

Auxier, J.D., Jordan, J.A., Stratz, S.A., Shahbazi, S., Hanson, D.E., Cressy, D. & Hall, H.L. 2016. Thermodynamic analysis of volatile organometallic fission products. *Journal of radioanalytical and nuclear chemistry*, 307(3):1621-1627.

Badaut, V., Wallenius, M. & Mayer, K. 2009. Anion analysis in uranium ore concentrates by ion chromatography. *Journal of Radioanalytical and Nuclear Chemistry*, 280(1):57-61.

Balatsky, G.I. & Severe, W.R. 2019. Illicit Trafficking of Radioactive and Nuclear Materials. In. *Nuclear Safeguards, Security, and Nonproliferation*: Elsevier. pp. 357-387.

Balboni, E., Simonetti, A., Spano, T., Cook, N.D. & Burns, P.C. 2017. Rare-earth element fractionation in uranium ore and its U (VI) alteration minerals. *Applied Geochemistry*, 87:84-92.

Bau, M., Schmidt, K., Koschinsky, A., Hein, J., Kuhn, T. & Usui, A. 2014. Discriminating between different genetic types of marine ferro-manganese crusts and nodules based on rare earth elements and yttrium. *Chemical Geology*, 381:1-9.

Bazilio, A. & Weinrich, J. 2012. The easy guide to: inductively coupled plasma-mass spectrometry (ICP-MS). Amherst: University of Massachusetts.

Borg, L. & Hutcheon, I. 2013. *Forensic analysis of samples from the nuclear fuel cycle*.

Boshielo, P. & Mogafe, R. 2015. *NECSA'S Need to Establish a Nuclear Forensics Specific NDA Facility for On-Site Categorization of Seized Nuclear Materials*.

Bradley, V.C., Manard, B.T., Roach, B.D., Metzger, S.C., Rogers, K.T., Ticknor, B.W., ... Hexel, C.R. 2020. Rare earth element determination in uranium ore concentrates using online and offline chromatography coupled to ICP-MS. *Minerals*, 10(1):55.

Brennecka, G.A., Borg, L.E., Hutcheon, I.D., Sharp, M.A. & Anbar, A.D. 2010. Natural variations in uranium isotope ratios of uranium ore concentrates: Understanding the 238U/235U fractionation mechanism. *Earth and Planetary Science Letters*, 291(1-4):228-233.

Brito, P., Caetano, M., Martins, M.D. & Caçador, I. 2021. Effects of salt marsh plants on mobility and bioavailability of REE in estuarine sediments. *Science of The Total Environment*, 759:144314.

Bryan, J.C. 2018. *Introduction to nuclear science*. CRC press.

Bull, T. & Smith, D.K. 2015. IAEA Coordinated Research Project: Application of Nuclear Forensics in Combating Illicit Trafficking of Nuclear and Other Radioactive Material. In. Advances in Nuclear

Forensics: Countering the Evolving Threat of Nuclear and Other Radioactive Material out of Regulatory Control. Proceedings of an International Conference. Companion CD-ROM.
Cates, N.L., Ziegler, K., Schmitt, A.K. & Mojzsis, S.J. 2013. Reduced, reused and recycled: Detrital zircons define a maximum age for the Eoarchean (ca. 3750–3780 Ma) Nuvvuagittuq Supracrustal Belt, Québec (Canada). *Earth and Planetary Science Letters*, 362:283-293.
Chen, J., Wei, M., Liu, X. & Wang, J. 2012. Back-end of nuclear fuel cycle in China. *Progress in Nuclear Energy*, 54(1):46-48.
Chen, J., Li, K., Chang, K.-J., Sofia, G. & Tarolli, P. 2015. Open-pit mining geomorphic feature characterisation. *International Journal of Applied Earth Observation and Geoinformation*, 42:76-86.
Collum, B. 2016. *Nuclear Facilities: A Designer's Guide*. Woodhead Publishing.
Commission, U.S.N.R. 2020. *Uranium enrichment*. https://www.nrc.gov/materials/fuel-cycle-fac/ur-enrichment.html Date of access: 15 November 2022.
Connelly, L.M. 2021. Introduction to analysis of variance (ANOVA). *Medsurg Nursing*, 30(3):218-158.
Corcoran, L., Simonetti, A., Spano, T.L., Lewis, S.R., Dorais, C., Simonetti, S. & Burns, P.C. 2019. Multivariate analysis based on geochemical, isotopic, and mineralogical compositions of uranium-rich samples. *Minerals*, 9(9):537.
Crossland, I. 2012. *Nuclear fuel cycle science and engineering*. Elsevier.
Dai, S., Seredin, V.V., Ward, C.R., Hower, J.C., Xing, Y., Zhang, W., ... Wang, P. 2015. Enrichment of U–Se–Mo–Re–V in coals preserved within marine carbonate successions: geochemical and mineralogical data from the Late Permian Guiding Coalfield, Guizhou, China. *Mineralium Deposita*, 50(2):159-186.
Dasnois, N. 2012. Uranium mining in Africa: a continent at the centre of a global nuclear renaissance.
do AMARAL, C., Machado, R.C., BARROS, J.d.A., Virgilio, A., Schiavo, D., NOGUEIRA, A.d.A. & NOBREGA, J.d.A. 2016. Determination of rare earth elements in geological samples using the agilent SVDV ICP-OES. In. Embrapa Pecuária Sudeste-Artigo em anais de congresso (ALICE). In: WINTER CONFERENCE ON PLASMA SPECTROCHEMISTRY, 2016, Tucson, Arizona ….
Donard, A., Pottin, A.-C., Pointurier, F. & Pécheyran, C. 2015. Determination of relative rare earth element distributions in very small quantities of uranium ore concentrates using femtosecond UV laser ablation–SF-ICP-MS coupling. *Journal of Analytical Atomic Spectrometry*, 30(12):2420-2428.
Downes, R., Hobbs, C. & Salisbury, D. 2019. Combating nuclear smuggling? Exploring drivers and challenges to detecting nuclear and radiological materials at maritime facilities. *The Nonproliferation Review*, 26(1-2):83-104.
Edwards, C. & Oliver, A. 2000. Uranium processing: a review of current methods and technology. *Jom*, 52(9):12-20.
Eichholz, G.G. & Poston, J.W. 2018. *Principles of nuclear radiation detection*. CRC Press.
El-Gamal, H. & El-Haddad, M. 2019. Estimation of natural radionuclides and rare earth elements concentration of the rocks of Abu Khuruq ring complex, Egypt. *Symmetry*, 11(8):1041.
El Bahariya, G.A. 2019. Geochemistry and tectonic setting of Neoproterozoic rocks from the Arabian-Nubian shield: emphasis on the Eastern Desert of Egypt. In. *Applied Geochemistry with Case Studies on Geological Formations, Exploration Techniques and Environmental Issues*: IntechOpen.
Emerson, R.W. 2019. Unpacking ANOVA Reporting. *Journal of Visual Impairment & Blindness*, 113(5):473-475.
Erpenbeck, H.H. 2017. *Safeguarding the nuclear fuel cycle: mining, milling, and conversion*.
Falster, A.U., Simmons, W.B., Webber, K.L. & Boudreaux, A.P. 2018. Mineralogy and Geochemistry of the Erongo Sub-Volcanic Granite-Miarolitic-Pegmatite Complex, Erongo, NamibiaMiarolitic Pegmatites, Erongo. *The Canadian Mineralogist*, 56(4):425-449.
Freire, G. & Cota, R. 2017. Capture of images in inaccessible areas in an underground mine using an unmanned aerial vehicle. In. Proceedings of the First International Conference on Underground Mining Technology. Australian Centre for Geomechanics.
Grove, S.K., Burns, N. & Gray, J. 2012. *The practice of nursing research: Appraisal, synthesis, and generation of evidence*. Elsevier Health Sciences.

Guenther, R., Lowenthal, M., Nagappa, R. & Mancheri, N. 2013. *India-United States cooperation on global security: Summary of a workshop on technical aspects of civilian nuclear materials security*. National Academies Press.
Gupta, C. & Singh, H. 2003. *Uranium resource processing: secondary resources*. Springer Science & Business Media.
Han, S.-H., Varga, Z., Krajkó, J., Wallenius, M., Song, K. & Mayer, K. 2013. Measurement of the sulphur isotope ratio (34 S/32 S) in uranium ore concentrates (yellow cakes) for origin assessment. *Journal of Analytical Atomic Spectrometry*, 28(12):1919-1925.
Harwood, L.M. 2012. Handbook of Radioactivity Analysis; edited by Michael.
Hiess, J., Condon, D.J., McLean, N. & Noble, S.R. 2012. 238U/235U systematics in terrestrial uranium-bearing minerals. *Science*, 335(6076):1610-1614.
Ho, D.M.L. 2015. *Study on the applicability of structural and morphological parameters on selected uranium compounds for nuclear forensic purposes.*
Hore-Lacy, I. 2016. Uranium for nuclear power: Resources, mining and transformation to fuel.
Jarding, L.J. 2011. Uranium Activities' Impacts on Lakota Territory. *Indigenous Policy Journal*, 22(2),
Jariwala, K.N. 2014. Nuclear Forensics-A Review.
John, S., Usman, I., Akpa, T. & Ibrahim, U. 2021. Rare earth elements in Uranium ore for nuclear forensic application. In. IOP Conference Series: Earth and Environmental Science. IOP Publishing. p 012075.
Kamunda, C., Mathuthu, M. & Madhuku, M. 2016a. Health risk assessment of heavy metals in soils from Witwatersrand Gold Mining Basin, South Africa. *International Journal of Environmental Research and Public Health*, 13(7):663.
Kamunda, C., Mathuthu, M. & Madhuku, M. 2016b. An assessment of radiological hazards from gold mine tailings in the province of Gauteng in South Africa. *International Journal of environmental research and public health*, 13(1):138.
Keatley, A., Scott, T., Davis, S., Jones, C. & Turner, P. 2015. An investigation into heterogeneity in a single vein-type uranium ore deposit: Implications for nuclear forensics. *Journal of environmental radioactivity*, 150:75-85.
Keegan, E., Wallenius, M., Mayer, K., Varga, Z. & Rasmussen, G. 2012. Attribution of uranium ore concentrates using elemental and anionic data. *Applied geochemistry*, 27(8):1600-1609.
Keegan, E., Kristo, M.J., Toole, K., Kips, R. & Young, E. 2016. Nuclear forensics: scientific analysis supporting law enforcement and nuclear security investigations. ACS Publications.
Keegan, E., Kristo, M.J., Colella, M., Robel, M., Williams, R., Lindvall, R., ... Gaffney, A. 2014. Nuclear forensic analysis of an unknown uranium ore concentrate sample seized in a criminal investigation in Australia. *Forensic science international*, 240:111-121.
Kennedy, A., Bostick, D., Hexel, C., Smith, R. & Giaquinto, J. 2013. Non-volatile organic analysis of uranium ore concentrates. *Journal of Radioanalytical and Nuclear Chemistry*, 296(2):817-821.
Khumalo, N. 2017. *Application of ICP-MS ahd Isotopic Techniques in Resolving Nuclear Forensic Signatures in Uranium Mining and Processing.* North-West University (South-Africa).
Khumalo, N. & Mathuthu, M. 2018. Determination of trace elements and lanthanide (REE) signatures in uranium mine products in South Africa by means of inductively coupled plasma mass spectrometry. *Journal of Geochemical Exploration*, 186:235-242.
Ko, W.I. & Gao, F. 2012. Economic analysis of different nuclear fuel cycle options. *Science and Technology of Nuclear Installations*, 2012,
Krajko, J. 2016. Isotopic signatures for origin assessment of natural uranium samples.
Krajkó, J., Varga, Z., Yalcintas, E., Wallenius, M. & Mayer, K. 2014. Application of neodymium isotope ratio measurements for the origin assessment of uranium ore concentrates. *Talanta*, 129:499-504.
Krajkó, J., Varga, Z., Wallenius, M., Mayer, K. & Konings, R. 2016. Investigation of sulphur isotope variation due to different processes applied during uranium ore concentrate production. *Journal of radioanalytical and nuclear chemistry*, 309(3):1113-1121.
Kristo, M. 2011. *Nuclear Forensics in Radiometric Methods of Detection*.

Kristo, M.J. 2020. Nuclear forensics. In. *Handbook of Radioactivity Analysis: Volume 2*: Elsevier. pp. 921-951.
Kristo, M.J. & Tumey, S.J. 2013. The state of nuclear forensics. *Nuclear Instruments and Methods in Physics Research Section B: Beam Interactions with Materials and Atoms*, 294:656-661.
Kristo, M.J., Gaffney, A.M., Marks, N., Knight, K., Cassata, W.S. & Hutcheon, I.D. 2016. Nuclear forensic science: analysis of nuclear material out of regulatory control. *Annual review of earth and planetary sciences*, 44:555-579.
Kritsananuwat, R., Sahoo, S.K., Fukushi, M. & Chanyotha, S. 2015. Distribution of rare earth elements, thorium and uranium in Gulf of Thailand's sediments. *Environmental Earth Sciences*, 73(7):3361-3374.
L'Annunziata, M.F. 2012. *Handbook of radioactivity analysis*. Academic press.
Laili, Z., Husain, H., Azman, M.A. & Paulus, W.S. 2020. Role of Nuclear Forensic Signatures in Supporting the Investigation of the Orphan Radioactive Source. *Jurnal Sains Nuklear Malaysia*, 32(1):58-64.
Lilley, J. 2013. *Nuclear physics: principles and applications*. John Wiley & Sons.
Lina, M., Zhaoa, Y., Wanga, T., Zhua, L. & Zhaoa, X. 2014. Attribution of uranium ore concentrates (UOCs) by rare-earth element (REE) signatures.
Liu, X.-M., Hardisty, D.S., Lyons, T.W. & Swart, P.K. 2019. Evaluating the fidelity of the cerium paleoredox tracer during variable carbonate diagenesis on the Great Bahamas Bank. *Geochimica et Cosmochimica Acta*, 248:25-42.
Madzunya, D., Uushona, V., Mathuthu, M. & Heike, W. 2021. Rare earth elements in uranium ore deposits from Namibia: A nuclear forensics tool. *Journal of Environmental Radioactivity*, 237:106668.
Malley, M.C. 2011. *Radioactivity: a history of a mysterious science*. Oxford University Press.
Manzi, M., Cooper, G., Malehmir, A., Durrheim, R. & Nkosi, Z. 2015. Integrated interpretation of 3D seismic data to enhance the detection of the gold-bearing reef: Mponeng Gold mine, Witwatersrand Basin (South Africa). *Geophysical Prospecting*, 63(4-Hard Rock Seismic imaging):881-902.
Martin, A. 2012. Radioactivity and radiation. In. *An Introduction to Radiation Protection 6E*: CRC Press. pp. 16-27.
Martin, B.R. & Shaw, G. 2019. *Nuclear and particle physics: an introduction*. John Wiley & Sons.
Mathuthu, M. & Khumalo, N. 2017. Developing nuclear forensics signatures and national nuclear forensics libraries for the African continent: A case review for South Africa. *International Journal of Applied Science-Research and Review*, 4(1):1-3.
Mathuthu, M., Khumalo, N., Baloyi, M. & Maretela, R. 2017. *Resolving Nuclear Forensic Signatures from a Uranium and Thorium Mine in South Africa Using the ICP-MS Isotopic Ratio Technique*.
Mayer, K., Wallenius, M. & Varga, Z. 2013. Nuclear forensic science: correlating measurable material parameters to the history of nuclear material. *Chemical reviews*, 113(2):884-900.
Melanofthalmidou, G., Lantzos, I. & Nicolaou, G. 2015. Identification of Unknown Nuclear Material.
Mercadier, J., Cuney, M., Lach, P., Boiron, M.C., Bonhoure, J., Richard, A., ... Kister, P. 2011. Origin of uranium deposits revealed by their rare earth element signature. *Terra Nova*, 23(4):264-269.
Mishra, P., Singh, U., Pandey, C.M., Mishra, P. & Pandey, G. 2019. Application of student's t-test, analysis of variance, and covariance. *Annals of cardiac anaesthesia*, 22(4):407.
Mogafe, R. & Chakrov, P. 2015. Co-Chairs' Summary of Technical Session 3E. Confidence in Nuclear Forensic Findings. In. Advances in Nuclear Forensics: Countering the Evolving Threat of Nuclear and Other Radioactive Material out of Regulatory Control. Summary of an International Conference.
Moody, K.J., Grant, P.M. & Hutcheon, I.D. 2014. *Nuclear forensic analysis*. CRC Press.
Murchie, M.P. & Reid, S.J. 2020. Uranium conversion and enrichment. In. *Advances in Nuclear Fuel Chemistry*: Elsevier. pp. 331-370.
Nash, K.L. & Lumetta, G.J. 2011. *Advanced separation techniques for nuclear fuel reprocessing and radioactive waste treatment*. Elsevier.
Ntsohi, L. 2019. *Characterization of uranium mined ore for nuclear forensic applications.*

Ntsohi, L., Usman, I., Mavunda, R. & Kureba, O. 2021. Characterization of uranium in soil samples from a prospective uranium mining in Serule, Botswana for nuclear forensic application. *Journal of Radiation Research and Applied Sciences*, 14(1):23-33.
Nwaila, G., Bourdeau, J., Jinnah, Z., Frimmel, H., Bybee, G., Zhang, S., ... Mashaba, D. 2021. The Significance of Erosion Channels on Gold Metallogeny in the Witwatersrand Basin (South Africa): Evidence from the Carbon Leader Reef in the Carletonville Gold Field. *Economic Geology*, 116(2):265-284.
Pajo, L., Mayer, K. & Koch, L. 2001. Investigation of the oxygen isotopic composition in oxidic uranium compounds as a new property in nuclear forensic science. *Fresenius' journal of analytical chemistry*, 371(3):348-352.
Park, B.H., Gao, F., Kwon, E.-h. & Ko, W.I. 2011. Comparative study of different nuclear fuel cycle options: Quantitative analysis on material flow. *Energy Policy*, 39(11):6916-6924.
Patah, M., Shafiee, N., Ismail, R., Bahar, A., Khan, M., Rak, A.E. & Awang, M. 2021. Distribution of light (LHREE) and heavy rare earth elements (HREE) in Kelantan granitoids rock. In. IOP Conference Series: Earth and Environmental Science. IOP Publishing. p 012038.
Peiró, L.T. & Méndez, G.V. 2013. Material and energy requirement for rare earth production. *JOM*, 65(10):1327-1340.
Peńkin, M., Boulyga, S. & Fischer, D. 2016. Application of uranium impurity data for material characterization in nuclear safeguards. *Journal of Radioanalytical and Nuclear Chemistry*, 307(3):1995-1999.
Piro, M.H. & Lipkina, K. 2020. Mining and milling. In. *Advances in Nuclear Fuel Chemistry*: Elsevier. pp. 315-329.
Polit, D. & Beck, C. 2020. *Essentials of nursing research: Appraising evidence for nursing practice*. Lippincott Williams & Wilkins.
Reading, D.G. 2016. *Nuclear forensics: determining the origin of uranium ores and uranium ore concentrates via radiological, elemental and isotopic signatures.* University of Southampton.
Schwerdt, I.J., Olsen, A., Lusk, R., Heffernan, S., Klosterman, M., Collins, B., ... McDonald IV, L.W. 2018. Nuclear forensics investigation of morphological signatures in the thermal decomposition of uranyl peroxide. *Talanta*, 176:284-292.
Shafiee, N.S., Bahar, A.M.A. & Khan, M.M.A. 2020. Potential of Rare Earth Elements (REEs) in Gua Musang Granites, Gua Musang, Kelantan. In. IOP Conference Series: Earth and Environmental Science. IOP Publishing. p 012027.
Silvennoinen, P. 2013. *Nuclear fuel cycle optimization: methods and modelling techniques*. Elsevier.
Spano, T.L., Simonetti, A., Wheeler, T., Carpenter, G., Freet, D., Balboni, E., ... Burns, P.C. 2017. A novel nuclear forensic tool involving deposit type normalized rare earth element signatures. *Terra Nova*, 29(5):294-305.
Srncik, M.B. 2011. *Investigation of the 236U occurrence in the environment.* uniwien.
Stanley, F.E., Stalcup, A. & Spitz, H. 2013. A brief introduction to analytical methods in nuclear forensics. *Journal of Radioanalytical and Nuclear Chemistry*, 295(2):1385-1393.
Straub, M.D., Arnold, J., Fessenden, J. & Kiplinger, J.L. 2020. Recent Advances in Nuclear Forensic Chemistry. *Analytical Chemistry*,
Švedkauskaitė-Le Gore, J. 2008. Development and validation of a method for origin determination of uranium-bearing material.
Swinney, M.W. 2015. *Experimental and Computational Assessment of Trace Nuclide Ratios in Weapons Grade Plutonium for Nuclear Forensics Analysis.*
Tamasi, A.L., Cash, L.J., Eley, C., Porter, R.B., Pugmire, D.L., Ross, A.R., ... Walensky, J.R. 2016. A lexicon for consistent description of material images for nuclear forensics. *Journal of Radioanalytical and Nuclear Chemistry*, 307(3):1611-1619.
Tucker, R.F., Viljoen, R.P. & Viljoen, M.J. 2016. A review of the Witwatersrand Basin–The world's greatest goldfield. *Episodes*, 39(2):5-33.

Vajda, N. & Kim, C.-K. 2011. Determination of transuranium isotopes (Pu, Np, Am) by radiometric techniques: a review of analytical methodology. *Analytical chemistry*, 83(12):4688-4719.
Varga, Z., Wallenius, M. & Mayer, K. 2010. Origin assessment of uranium ore concentrates based on their rare-earth elemental impurity pattern. *Radiochimica Acta*, 98(12):771-778.
Varga, Z., Wallenius, M., Mayer, K. & Meppen, M. 2011. Analysis of uranium ore concentrates for origin assessment. *Proceedings in Radiochemistry*, 1(1):27-30.
Varga, Z., Nicholl, A., Wallenius, M. & Mayer, K. 2012. Development and validation of a methodology for uranium radiochronometry reference material preparation. *Analytica chimica acta*, 718:25-31.
Varga, Z., Wallenius, M., Mayer, K., Keegan, E. & Millet, S. 2009. Application of lead and strontium isotope ratio measurements for the origin assessment of uranium ore concentrates. *Analytical chemistry*, 81(20):8327-8334.
Vesterlund, A. 2019. *Method Development for Signatures in Nuclear Material for Nuclear Forensic Purposes*. Chalmers Tekniska Hogskola (Sweden).
Walther, C. & Wendt, K. 2020. Radioisotope mass spectrometry. In. *Handbook of Radioactivity Analysis*: Elsevier. pp. 861-898.
Wang, L. & Liang, T. 2015. Geochemical fractions of rare earth elements in soil around a mine tailing in Baotou, China. *Scientific reports*, 5(1):1-11.
Weyer, S., Anbar, A., Gerdes, A., Gordon, G., Algeo, T. & Boyle, E. 2008. Natural fractionation of 238U/235U. *Geochimica et Cosmochimica Acta*, 72(2):345-359.
Wilson, P.D. & Krauskopf, K.B. 1997. The Nuclear Fuel Cycle, from Ore to Waste. *Economic Geology and the Bulletin of the Society of Economic Geologists*, 92(3):380-381.
Zepf, V. 2013. Rare Earth Elements: What and where they are. In. *Rare earth elements*: Springer. pp. 11-39.
Zhou, Y., Li, G., Xu, L., Liu, J., Sun, Z. & Shi, W. 2020. Uranium recovery from sandstone-type uranium deposit by acid in-situ leaching-an example from the Kujieertai. *Hydrometallurgy*, 191:105209.
Zhu, Z. & Cheng, C.Y. 2011. A review of uranium solvent extraction: its present status and future trends.
Zhuang, M., Zhao, J., Li, S., Liu, D., Wang, K., Xiao, P., ... Zhou, J. 2017. Concentrations and health risk assessment of rare earth elements in vegetables from mining area in Shandong, China. *Chemosphere*, 168:578-582.